

1 **Direct and indirect effects of joint torque inputs during an induced speed analysis of a swinging motion**

2
3 **Accepted in Journal of Biomechanics, 17/01/2019**

4
Sekiya Koike¹, Tatsuya Ishikawa², Alexander P. Willmott³ and Neil Bezodis⁴

¹Faculty of Health and Sport Sciences, University of Tsukuba, Japan,

²Institute of Sport Science, Asics Corporation, Japan

³School of Sport and Exercise Science, University of Lincoln, UK

⁴Applied Sports, Technology, Exercise and Medicine Research Centre, Swansea University, UK

Corresponding Author:

Sekiya Koike, Faculty of Health and Sport Sciences, University of Tsukuba,

1-1-1 Tennodai, Tsukuba City, Ibaraki Prefecture, 305-8574, Japan.

Tel: +81 – 29 – 853 – 2677

Fax: +81 – 29 – 853 – 2677

E-mail: koike.sekiya.fp@u.tsukuba.ac.jp

5
6 **Keywords:**

7 Kinetic chain, Whip-like effect, Dynamic contribution, Cause-and-effect relationship, Rugby kicking

8 **Word Count:** 3997 in manuscript, and 1739 in appendices for supplementary

9 **Abstract**

10 This study proposed a method to quantify direct and indirect effects of the joint torque inputs in the speed-generating
11 mechanism of a swinging motion. Linear and angular accelerations of all segments within a multi-linked system can
12 be expressed as the sum of contributions from a joint torque term, gravitational force term and motion-dependent term
13 (MDT), where the MDT is a nonlinear term consisting of centrifugal force, Coriolis force and a gyroscopic effect
14 moment. Direct effects result from angular accelerations induced by a joint torque at a given instant, whereas indirect
15 effects arise through the MDT induced by joint torques exerted in the past. These two effects were quantified for the
16 kicking-side leg during a rugby place kick. The MDT was the largest contributor to the foot centre of gravity (CG)'s
17 speed at ball contact. Of the factors responsible for generating the MDT, the direct and indirect effects of the hip
18 flexion-extension torque during both the flight phase (from the final kicking foot take-off to support foot contact) and
19 the subsequent support phase (from support foot contact to ball contact) were important contributors to the foot CG's
20 speed at ball contact. The indirect effect of the ankle plantar-dorsal flexion torque and the direct effect of the knee
21 flexion-extension torque during the support phase showed the largest positive and negative contributions to the foot
22 CG's speed at ball contact, respectively. The proposed method allows the identification of which individual joint
23 torque axes are crucial and the timings of joint torque exertion that are used to generate a high speed of the distal point
24 of a multi-linked system.

25 **NOMENCLATURE**

26 \mathbf{V} generalised velocity vector consisting of linear and angular velocity vectors for all the segments

27 $\dot{\mathbf{V}}$ generalised acceleration vector

28 $\mathbf{A}_{\mathbf{V},\mathbf{T}_a}$ coefficient matrix for the joint torque vector

29 \mathbf{T}_a joint torque vector consisting of active torques

30 $\bar{\mathbf{A}}_{\mathbf{V},\text{MDT}}(\mathbf{V})$ coefficient matrix for the motion-dependent term, which is a function of the generalised velocity vector

31 $\mathbf{A}_{\mathbf{V},\mathbf{G}}$ coefficient matrix for gravitational force

32 \mathbf{G} gravitational force vector

33 $\mathbf{B}_{\mathbf{V},\text{other}}$ vector consisting of the hip-joint acceleration, segment length fluctuation, and constraint joint axial angle

34 fluctuation terms

35 $\mathbf{A}_{\mathbf{V},\text{Hip}}$ coefficient matrix for the hip joint acceleration vector

36 $\ddot{\mathbf{x}}_{\text{Hip}}$ hip joint acceleration

37 $\mathbf{A}_{\mathbf{V},\boldsymbol{\eta}}$ coefficient matrix for the double derivation of segment length fluctuation vector

38 $\boldsymbol{\eta}$ vector of segment length fluctuation

39 $\mathbf{A}_{\mathbf{V},\boldsymbol{\varphi}}$ coefficient matrix for the double derivation of constraint joint axial angle fluctuation

40 $\boldsymbol{\varphi}$ vector of constraint joint axial angle fluctuation

41 $\dot{\mathbf{V}}_{\text{Dir}}$ generalised acceleration vector due to the direct effect of joint torque, gravity and other inputs

42 $\dot{\mathbf{V}}_{\text{Indir}}$ generalised acceleration vector due to the indirect effect of joint torque, gravity and other inputs

43 k k -th time instant in the discrete-time system

44 h any given instant in time between swing start to time k

45	Δt	time interval in the discrete-time system
46	Ψ_V	coefficient matrix for the generalised velocity vector defined as $\mathbf{E}_{18} + \Delta t \bar{\mathbf{A}}_{V,MDT}(\mathbf{V})$
47	\mathbf{E}_{18}	unit matrix with eighteen rows and columns
48	$\tilde{\mathbf{V}}$	measured generalised velocity vector
49	$\tilde{\Psi}_V$	coefficient matrix for the generalised velocity vector defined as $\mathbf{E}_{18} + \Delta t \bar{\mathbf{A}}_{V,MDT}(\tilde{\mathbf{V}})$
50	$\mathbf{V}(0)$	initial value of the generalised velocity vector
51	i	subscript expressing segment number (i.e. $i=1$, thigh; $i=2$, shank; $i=3$, foot)
52	\mathbf{S}_i	selective matrix extracting the linear velocity vector of segment i from the generalised velocity vector
53	$\dot{\mathbf{x}}_i$	linear velocity vector for the centre of gravity of segment i
54	\mathbf{e}_i	unit vector for the linear velocity vector for the centre of gravity of segment i
55	s_{Dir}	speed of segment's centre of gravity induced by direct effect of joint torque inputs
56	s_{Indir}	speed of segment's centre of gravity induced by indirect effect of joint torque inputs
57	s_i	contribution to the speed of segment i 's centre of gravity induced by both direct and indirect effects of joint
58		torque inputs

59 1. Introduction

60 Quantification of the kinetics underpinning the generation of high distal-point speed in swinging motions has provided
61 knowledge regarding how players exert joint torques to produce distinctive patterns of motion within a multi-linked
62 system. Numerous studies have analysed high-speed swinging motions such as baseball pitching (e.g. Feltner and
63 Dapena, 1986; Feltner, 1989; Fleisig et al., 1995; Fleisig et al., 1996a; Fleisig et al., 1996b), tennis serving (e.g. Elliott
64 et al., 2003; Reid et al., 2007), and soccer kicking (e.g. Lees and Rahnama, 2013; Nunome et al., 2002). Although
65 these studies reveal how players exert joint torques during these motions, it remains unclear exactly how and when the
66 individual joint torques exerted affect the speed of the multi-linked system at ball release or ball contact, because such
67 kinetic analyses have limitations in dealing with the cause-and-effect relationship between joint torque inputs and
68 motion outputs.

69 Since the human body consists of numerous segments connected via joints which are typically assumed to move
70 with only rotational displacements, human movements are performed through angular displacements at joints to
71 achieve coordinated multiple segment motion. The equation of motion for a multi-linked system (e.g. human body)
72 can be expressed generally in the following form (e.g. Kepple et al., 1997; Koike et al., 2017; Zajac et al., 2002) when
73 ignoring modelling errors:

$$\begin{aligned} & \text{(Linear and angular accelerations of all segments) or (Angular accelerations of all joints)} \\ & = \text{(Joint torque term)} + \text{(Gravitational term)} + \text{(Motion-dependent term)}, \end{aligned} \tag{1}$$

74 where the motion-dependent term (MDT) is a nonlinear term consisting of centrifugal forces, Coriolis forces and
75 gyroscopic effect moments. Equation 1 indicates that segmental motion (i.e. linear and angular accelerations) is
76 induced not only by the joint torque inputs and gravitational force but also by the MDT. Motion can be induced by the

77 joint forces exerted at individual joints through motion-dependent mechanisms, even when the inputted joint torques
78 are small. These joint forces do not appear directly as a separate term in Equation 1 because they are not a primary
79 source like joint torques or gravity but are a secondary source included in the motion-dependent effects arising from
80 the primary sources.

81 The MDT plays a crucial role in the generation of angular accelerations that influence distal-point speed in
82 high-speed swinging motions (Hirashima, 2008; Hirashima et al., 2008; Koike and Harada, 2014; Koike and Mimura,
83 2016a, 2016b; Naito and Maruyama, 2008; Naito et al., 2017; Putnam, 1991). Since the MDT is caused by product
84 sums of angular velocities of individual segments, the MDT contribution will be relatively large when angular
85 velocities of several segments increase before ball release or ball contact. The angular velocities of individual
86 segments, caused by earlier joint torques, produce centrifugal and Coriolis forces, and thus the entire joint torque
87 time-histories must be considered when investigating the MDT. At any given instant, previously applied joint torques
88 can still exert an indirect effect on system behaviour through a mechanism sometimes called the “cumulative effect”
89 of joint torque inputs (Zajac et al., 2003; Hirashima et al., 2008; Hirashima, 2008) or “whip-like effect” (Atwater,
90 1979; Feltner, 1989; Fleisig et al., 1996; Kibler, 1995; Kindall, 1992; Putnam, 1991). However, the contributions of
91 these indirect effects to the generation of segmental speeds have not previously been quantified during any swinging
92 motions. In place of quantifying these indirect effects of joint torque inputs, an analysis decomposing the MDT into
93 kinematic sources (Hirashima et al., 2008; Naito et al., 2010; Naito et al., 2017) has been implemented to explain how
94 the components generate speed. However, this analysis does not reveal which axis of each joint torque is crucial, or
95 the time(s) at which a given joint torque is effective in contributing to the generation of a high distal-point speed.
96 Greater understanding of how each joint torque contributes to speed generation through these indirect effects is still

needed. A conversion algorithm that quantifies the generating factors of the MDT has been introduced briefly (Koike and Harada, 2014), but without detailed methods, and was applied to high-speed swinging motions including the tennis serve (Koike and Harada, 2014), baseball batting (Koike and Mimura, 2016b), rugby place kicking (Koike and Bezodis, 2017), and baseball pitching (Koike, Uzawa and Hirayama, 2018). Although the factors contributing to the generation of the distal-point speed were examined for these motions, the direct and indirect effects of the joint torque inputs were not separately quantified.

The objectives of this study were to: (1) propose and describe a method which separately quantifies the direct and indirect effects of joint torques to the generation of distal-point speed in a multi-linked system; and (2) illustrate how the direct and indirect contributions differ in an example high-speed swinging motion: a rugby place kick.

2. Methods

2.1. Equation of motion for a multi-linked system

Since the equation of motion for a multi-linked system includes a cause-and-effect relationship between joint torque inputs and motion outputs, the general equation of motion (Equation 1) was used to derive a recurrence formula which can take the indirect effect of joint torque inputs into account. The proposed method was applied to the kicking-side lower limb segments during a rugby place kick.

The dynamical equation for the kicking-side leg, consisting of thigh, shank and foot segments, can be expressed as follows (see Appendix 1 for details):

$$\dot{\mathbf{V}} = \mathbf{A}_{V,Ta} \mathbf{T}_a + \bar{\mathbf{A}}_{V,MDT}(\mathbf{V})\mathbf{V} + \mathbf{A}_{V,G} \mathbf{G} + \mathbf{B}_{V,other} \quad (2)$$

where the vector \mathbf{V} denotes the generalised velocity vector $\mathbf{V} = [\dot{\mathbf{x}}_1^T \ \boldsymbol{\omega}_1^T \ \dot{\mathbf{x}}_2^T \ \boldsymbol{\omega}_2^T \ \dot{\mathbf{x}}_3^T \ \boldsymbol{\omega}_3^T]^T$, which consists of the

116 linear velocity vector $\dot{\mathbf{x}}_i$ and angular velocity vector $\boldsymbol{\omega}_i$ of all segments (where subscript i denotes segment number:
 117 $i=1$, thigh; $i=2$, shank; $i=3$, foot). The terms on the right-hand-side of Equation 2 represent the respective contributions
 118 to the generation of the generalised velocity vector of the joint torque term, motion-dependent term, gravitational term,
 119 and a term consisting of all the remaining sources with the matrices $\mathbf{A}_{V,Ta}$ and $\mathbf{A}_{V,G}$ indicating the coefficient matrices
 120 for the joint torque vector \mathbf{T}_a and gravitational force vector \mathbf{G} , $\bar{\mathbf{A}}_{V,MDT}(\mathbf{V})$ being the coefficient matrix associated
 121 with the MDT and $\mathbf{B}_{V,other}$ indicating the vector consisting of the remaining terms:

$$\mathbf{B}_{V,other} = \mathbf{A}_{V,Hip}\ddot{\mathbf{x}}_{Hip} + \mathbf{A}_{V,\eta}\ddot{\boldsymbol{\eta}} + \mathbf{A}_{V,\varphi}\ddot{\boldsymbol{\varphi}} \quad (3)$$

122 where the matrix $\mathbf{A}_{V,Hip}$ is the coefficient matrix for hip joint acceleration $\ddot{\mathbf{x}}_{Hip}$, the matrices $\mathbf{A}_{V,\eta}$ and $\mathbf{A}_{V,\varphi}$ are
 123 coefficient matrices for the vectors $\ddot{\boldsymbol{\eta}}$ and $\ddot{\boldsymbol{\varphi}}$, respectively (see Appendix 1 for more detail). These three terms on the
 124 right-hand side correspond to the hip joint acceleration, segment length fluctuation and anatomical constraint joint
 125 axial angle fluctuation terms, respectively.

126 Similarly to the combination of “instantaneous and cumulative acceleration vectors” in previous studies
 127 (Hirashima et al., 2008; Zajac et al, 2003), the generalised acceleration vector $\dot{\mathbf{V}}$ can be expressed as the sum of two
 128 types of acceleration vector:

$$\dot{\mathbf{V}} = \dot{\mathbf{V}}_{Dir} + \dot{\mathbf{V}}_{Indir}, \quad (4)$$

129 where $\dot{\mathbf{V}}_{Dir}$ denotes the acceleration vector due to the direct effect of joint torque, gravity and other inputs:

$$\dot{\mathbf{V}}_{Dir} = \mathbf{A}_{V,Ta}\mathbf{T}_a + \mathbf{A}_{V,G}\mathbf{G} + \mathbf{B}_{V,other}, \quad (5)$$

130 and $\dot{\mathbf{V}}_{Indir}$ denotes the acceleration vector due to the indirect effect of these inputs, mediated through
 131 motion-dependent processes arising from earlier direct effects:

$$\dot{\mathbf{V}}_{Indir} = \bar{\mathbf{A}}_{V,MDT}(\mathbf{V})\mathbf{V} \quad (6)$$

132 These relationships, expressed for a continuous-time system, can be represented with a block diagram (Figure 1).

133 ** Figure 1 near here **

134

135 2.2. Derivation of a recurrence formula with respect to the generalised velocity vector

136 The generalised acceleration vector can be expressed by difference approximation using the time interval Δt of the
137 discrete-time system shown as:

$$\dot{\mathbf{V}}(k) = \frac{\mathbf{V}(k+1) - \mathbf{V}(k)}{\Delta t} \quad (7)$$

138 After discretising Equations 4 to 6, combining Equations 4 to 7 yields a recurrence formula for the generalised
139 velocity vector \mathbf{V} as follows:

$$\mathbf{V}(k+1) = \Delta t \dot{\mathbf{V}}_{\text{Dir}}(k) + \Psi_{\mathbf{V}}(k)\mathbf{V}(k), \quad \Psi_{\mathbf{V}}(k) = \mathbf{E}_{18} + \Delta t \bar{\mathbf{A}}_{\mathbf{V},\text{MDT}}(\mathbf{V}(k)) \quad (8)$$

140 where \mathbf{E}_{18} is the unit matrix with eighteen rows and columns.

141 Since the coefficient matrix $\bar{\mathbf{A}}_{\mathbf{V},\text{MDT}}(\mathbf{V}(k))$ contains the angular velocity of the generalised velocity vector $\mathbf{V}(k)$
142 in its elements, the coefficient matrix $\Psi_{\mathbf{V}}(k)$ also contains the elements $\mathbf{V}(k)$. Although it is possible to numerically
143 obtain the states of the individual segments (e.g. linear and angular velocity vectors) for the individual input terms
144 using discretised Equations 5, 6 and 8, it would be impossible to calculate the indirect effect of the input terms using
145 these equations because Equation 8 is not a form of primary expression with respect to the vector $\mathbf{V}(k)$.

146 Thus, in order to quantify the indirect effect of the individual input terms, the generalised velocity vector $\mathbf{V}(k)$ in
147 the matrix $\bar{\mathbf{A}}_{\mathbf{V},\text{MDT}}(\mathbf{V}(k))$ in Equation 8 must be replaced with the generalised velocity vector $\tilde{\mathbf{V}}(k)$ measured at the
148 k -th time instant:

$$\mathbf{V}(k+1) = \Delta t \dot{\mathbf{V}}_{\text{Dir}}(k) + \tilde{\Psi}_{\mathbf{V}}(k)\mathbf{V}(k), \quad \tilde{\Psi}_{\mathbf{V}}(k) = \mathbf{E}_{18} + \Delta t \bar{\mathbf{A}}_{\mathbf{V},\text{MDT}}(\tilde{\mathbf{V}}(k)) \quad (9)$$

149 Since the vector $\tilde{\Psi}_V(k)V(k)$ has a form of primary expression with respect to the velocity vector $V(k)$, the recurrence
150 formula, Equation 9, can be expressed from the beginning of the motion to the k -th time instant of analysis (Figure
151 2a), and reshaped as shown in Figure 2b, where it becomes possible to quantify the total effect (i.e. direct and indirect
152 effects) of individual torque inputs to the generation of the generalised velocity vector.

153 Equations 5 and 9 can quantify the contributions of the individual input terms (i.e. the joint torque term, the
154 gravitational term, the hip-joint acceleration term, the segment length fluctuation term, and the anatomical constraint
155 joint axial angle fluctuation term) at time k to the generation of the generalised velocity vector at time $k+1$ considering
156 the generating factors of the MDT.

157 ** Figure 2 near here **

158 The total effects of joint torque inputs on the generation of the foot centre of gravity (CG) speed are expressed by a
159 block diagram (Figure 3a) consisting of the direct effect component (Figure 3b) and indirect effect component (Figure
160 3c).

161

162
163
164
165
166
167
168
169
170
171
172
173
174
175
176
177
178
179
180
181

** Figure 3 near here **

The direct and indirect effects of the individual joint torque inputs in generating the MDT can be quantified from Figure 3 (see Appendix 2 for details). The MDT contribution can be decomposed into kinematic components arising from centrifugal forces, Coriolis forces, gyroscopic effect moments and segmental length fluctuations (see Appendix 3 for details).

2.3. Data collection

Six male rugby players (two professional and four university-level; mean \pm SD of age: 21.9 \pm 1.8 years; height: 1.77 \pm 0.06 m; body mass: 81.8 \pm 4.4 kg) performed 5 - 8 place kicks. Each provided written informed consent, and study approval was obtained from the lead author's institution's ethics committee. The ball was placed on their preferred tee and kicked into a net approximately 4 m away. The kickers were instructed to kick as far and as straight (towards the centre of the net) as possible. Kinematic data (47 markers on the body, 6 on the ball) were recorded with a 14-camera motion capture system (VICON-MX, Vicon Motion Systems Ltd., Oxford, UK; 500 Hz). Kinetic data under the support leg were measured with a force platform (9287C, Kistler Inst.; 1000Hz). The kicking action was divided into two phases: flight and support. These were, respectively, the period from the final take-off of the kicking foot (KFO) to ground contact with the support foot (SFC), and the period from SFC to ball contact (BC). KFO was defined as when the kicking foot's 5th MTP marker first reached a vertical displacement of 0.10 m after its final ground contact prior to ball contact (Lees et al., 2009); SFC was based on a vertical ground reaction force threshold of

182 10 N, and BC was defined as the frame of peak anterior toe velocity (Shinkai et al., 2009). All data were
183 time-normalised to phase durations as -200% to -100% (flight, KFO to SFC) and -100% to 0% (support, SFC to BC).
184 Anatomical constraint axes (e.g. varus-valgus axis at knee joint; internal-external rotation axis at ankle joint) were also
185 considered in the modelling (Koike et al., 2017). The coordinate data were smoothed with a fourth-order
186 zero-phase-shift Butterworth low-pass digital filter whose optimal cut-off frequencies (5 - 15 Hz) were determined by
187 residual analysis (Wells and Winter, 1980). Three trials per participant were selected based on the participants' highest
188 subjective ratings, and the mean data across these trials were used for each participant.

190 **3. Results**

191 The flight and support phases lasted 0.11 ± 0.01 and 0.13 ± 0.01 seconds, respectively. The directly measured kicking
192 foot CG speed gradually increased until -60% (normalised) time, then increased rapidly toward BC, reaching
193 21.34 ± 0.70 m/s at BC (Figure 4a). The sum of the MDT and the contributions induced by the direct effect of
194 individual terms matched the measured foot CG's speed to within 0.19 m/s throughout the movement (Figures 4a to h).
195 Similarly, the total of the contributions induced by both the direct and indirect effects of individual terms, following
196 the partition of the MDT into its component indirect terms, also matched the measured foot CG's speed to within 0.14
197 m/s (Figures 4a, c to h).

198 The MDT was the dominant contributor to the foot CG's speed. The centrifugal force component accounted for
199 most of this MDT contribution (Figure 4b), but the Coriolis force component was also appreciable during the support
200 phase; the components relating to the gyroscopic effect moment and the segment length fluctuations were very small
201 throughout. The MDT's dynamic contribution increased gradually toward -95% time, then decreased until -50%,

202 before increasing rapidly toward BC where it reached 20.84 ± 3.67 m/s, or 98% of the foot CG's speed at this instant
203 (Figure 4b). After partitioning the MDT into its components, the total contribution from the direct effects of the
204 individual joint torque inputs increased until -35% time and then decreased toward BC, while the total indirect effects
205 of these inputs increased after -60% time toward BC (Figure 4c). The direct effect of the initial velocity term was
206 positive until -120% time and then became negative toward BC, whereas the indirect effect of the velocity term was
207 positive throughout, increasing until -90% time and then decreasing toward BC (Figure 4d). The contributions from
208 the direct and indirect effects of the gravitational force term, the hip joint acceleration term, the segment length
209 fluctuation term and the joint anatomical constraint axes fluctuation term were small (Figure 4e-h).

210 Consideration of the time derivatives of the direct and indirect effects associated with the torques for individual
211 joint rotations allows identification of the times when, and the specific axes about which, key contributions to the
212 kicking foot CG's speed at BC ($s_3(k_{BC})$; Figure 5) occurred. Peak positive contributions from the direct and indirect
213 effects of the hip flexion-extension torque occurred around -110 and -90% time, respectively (Figure 5a). The indirect
214 contributions from knee flexion-extension and ankle plantar-dorsiflexion torques were also positive (Figure 5d and f)
215 but these peaked slightly later (around -70% time). At this time, the direct effects of these knee and ankle torques were
216 large and negative (Figure 5d and f). Aside from the indirect effect of the ankle eversion-inversion torque, particularly
217 after SFC, the other non-sagittal plane torques made only small contributions throughout the entire movement (Figure
218 5b, c, e and g).

219 The integrated contribution across each phase to the foot CG's speed at BC was also determined for both the
220 direct and indirect effects of each individual axial torque (Figure 6a and b). The direct and indirect effects of the hip
221 flexion-extension torque contributed positively to the foot CG's speed at BC across both the flight phase and the

222 subsequent support phase. The indirect effects of the ankle plantar-dorsal flexion torques and the direct effects of the
223 knee flexion-extension torques, both across the support phase, showed the largest positive and negative contributions,
224 respectively.

225

226

** Figure 4 near here **

227

228

229

** Figure 5 near here **

230

231

** Figure 6 near here **

232

233

234

4. Discussion

235

This study firstly aimed to propose and describe a method which separately quantifies the direct and indirect effects of

236

joint torque inputs in the distal-point speed generation of a high-speed swinging motion. Secondly, we aimed to

237

illustrate how the model outputs differ between these direct and indirect effects, using a rugby place kick as an

238

example motion. The indirect effects of the joint torques, which are generated through motion-dependent processes as

239

a result of previously-exerted joint torques, were the largest contributor to the foot CG's speed at BC in this rugby

240

kicking motion (Figure 4c). Although the overall sum of the direct effects of joint torques showed only a small

241

contribution to the foot CG's speed at BC (Figure 4c), the direct effect of the hip flexion-extension torque (flexor

242

dominant throughout) was the major positive contributor to the foot CG's speed at BC, and this contributed during

243

both flight and support (Figures 6a and b). Interestingly, the indirect effects of the knee flexion-extension torque

244

(extensor dominant until -20%, then flexor dominant) and ankle plantar-dorsal flexion torque (dorsiflexor dominant

245

throughout) showed positive contributions, whereas the direct effects of those torques contributed negatively (Figures

246

5d and f, Figures 6a and b). Although exerting a knee extension torque would induce knee extension and therefore

247

contribute geometrically to the foot CG's speed, a negative direct contribution of knee extension torque to the foot

248 CG's speed was observed in this study. This non-intuitive phenomenon may be caused by the dynamic coupling (Kane
249 and Levinson, 1985) of the leg segments in which the knee extension torque would induce extension of hip joint, and
250 this hip extension would reduce the foot CG's speed, where dynamic coupling means that a torque input about one
251 joint axis can cause multi-axial angular accelerations of the body due to the non-diagonal inertial matrix of the
252 equation of motion for the system (Hirashima et al., 2007, 2008; Koike et al., 2017; Zajac et al., 2002, 2003). Further
253 investigation, using an induced joint angular velocity analysis, would be needed to verify this explanation. Since a
254 flexion torque was exerted about the hip joint throughout the movement and contributed positively to the foot CG's
255 speed via both direct and indirect effects, torque reversal – as found to be effective in Herring and Chapman's (1992)
256 simulation of a throwing motion – was not observed in this kicking motion. The relatively small effects of the hip joint
257 torques about the other axes (Figure 5b and 5c) support previous kinematic data which suggested that the contributions
258 of the hip adduction-abduction and internal-external rotation angular velocities to foot speed in rugby place kicking
259 are small (Zhang et al., 2012). Finally, the large contribution of the indirect effect of ankle plantar-dorsiflexion torques
260 to the foot CG's speed (Figures 5f and 6b) may be because the foot is swung with high speed around the shank and
261 thigh segments, and therefore this torque assists in effective orientation of the foot segment. This would help to control
262 the impact location between the foot and ball, which is an important feature for determining the ball flight
263 characteristics (Peacock and Ball, 2017). A similar effect was also evident in the ankle eversion-inversion torque
264 (Figure 5g and Figure 6b).

265 The method proposed in this study quantifies both the direct and indirect effects of individual joint torque inputs
266 in the generation of distal-point speed, and their use for evaluating performance, whereas previous studies showed
267 only the direct effect of joint torques in actions such as the generation of elbow extension angular velocity (Hirashima

268 et al., 2008; Naito and Maruyama, 2008), of distal-point speed (Naito et al., 2017), and of angular velocities about the
269 longitudinal axes of the upper arm and forearm segments (Naito et al., 2014) during overarm throwing and baseball
270 pitching, and in the generation of knee extension angular velocity during soccer kicking motion (Naito et al., 2010).
271 Although previous studies decompose the MDT into several components in order to describe how particular kinematic
272 features of segmental and joint movements affect the MDT contributions (e.g. Hirashima et al., 2008; Naito and
273 Maruyama, 2008; Naito et al., 2010; Naito et al., 2017; Putnam, 1991, 1993), kinematic analyses alone cannot reveal
274 the mechanisms by which these movements induce effective joint torques.

275 The capability of the algorithm to calculate the direct and indirect effects separately during the analysis of
276 high-speed swinging motions has been demonstrated. This approach can aid in the understanding of the specific
277 effects of individual joint torques exerted during swinging motions. For example, in rugby place kicking, high foot
278 speed at BC is required to achieve high ball launch velocities. In our analysis of the rugby place kick, the hip
279 flexion-extension torque exerted at around -110% time caused large foot CG speed at BC via the direct effect of the
280 torque, and the same axial torque exerted at around -90% time induced large foot CG speed at BC via the indirect
281 effect. Since the foot CG's speed induced solely by the direct effect of joint torques is limited by the force-producing
282 capacity of muscles crossing the joint, utilisation of the motion-dependent mechanisms is an effective strategy for
283 producing higher distal-point speeds during such a high-speed motion. Because the indirect effect of the hip
284 flexion-extension torque exerted around -90% time plays a significant role in the speed generation of the foot's CG at
285 BC by enhancing the contributions of the MDT prior to BC (Figures 5a and 6b), it is necessary to examine the direct
286 and indirect effects separately. The indirect effects of the knee flexion-extension and ankle plantar-dorsiflexion torques
287 peaked after the indirect effect of the hip flexion-extension torque, and the timing of these peaks (at approximately

288 -70% time) occurred close to where the centrifugal and Coriolis force components of the MDT inflected (Figure 4b).

289 While the ankle joint torque also plays a role via the indirect effect in the foot CG's speed generating mechanism

290 (Figure 5f), the role of the knee joint extension-flexion torque via the direct effect would be to prevent knee-joint

291 hyperextension (Apriantono et al., 2006; Dörge et al., 2002) and the role of the ankle plantar-dorsiflexion torque via

292 the direct effect may be to control the foot for accurate contact with the ball.

293 This study has presented the contributions to the kicking foot CG's speed using a model consisting only of the

294 kicking-side thigh, shank and foot segments. Since the current model consists of only these segments, the

295 contributions of joint torques other than the kicking-leg joint torques were not quantified. Thus, an analysis using a

296 whole-body model would be necessary to fully clarify the roles of all joint torques during rugby place kicking. A more

297 complete investigation of the whole-body kicking motion would require investigation of the contributions to the

298 angular velocities such as joint angular velocities and foot angular velocity using a whole-body model. However,

299 focusing on just the kicking leg is an appropriate starting point in understanding such complex high-speed swinging

300 motions, particularly given the primary aim of our study was to detail the model and demonstrate its potential. This

301 method can now be applied to any swinging motion, in a whole-body or part-body way, for a more complete

302 understanding of the distal-point speed generating mechanisms. Since this approach enables the effects of joint torque

303 inputs to be obtained even when the MDT plays a crucial role in the distal-point speed generation, estimation of

304 muscle force contributions can be performed by solving the load distribution problem with use of musculoskeletal

305 models (e.g. Delp et al., 2007).

306
307 **5. Conclusion**

308 A method for quantifying direct and indirect effects of joint torque inputs in the speed generating mechanism of a
309 swinging motion has been introduced, in which a direct effect is generated by angular accelerations induced by a joint
310 torque at a given instant, whereas an indirect effect is generated through a motion-dependent term (MDT: a nonlinear
311 term consisting of centrifugal force, Coriolis force and a gyroscopic effect moment) induced by earlier application of a
312 joint torque. The method allows identification of the individual joint torque axes and timings of joint torque exertion
313 that are used to generate a high speed of the distal point of a multi-linked system. The two types of effect were
314 quantified for joint torque inputs through a recurrence formula with respect to the generalised velocity vector of a
315 multi-linked system based on the equation of the system's motion including a cause-and-effect relationship between
316 joint torque inputs and motion outputs. The practical potential of this approach has been demonstrated through its
317 application to modelling the role of the kicking-side leg in generating foot speed during a rugby place kick. Important
318 contributions to foot CG speed, for example from the direct and indirect effects of the hip flexion-extension torque
319 during the flight phase and the subsequent support phase, were identified by considering the factors responsible for
320 generating the MDT. Further investigation will be needed to determine both direct and indirect effects for whole-body
321 joint torque inputs in the generation of distal-point speed in swinging motions.

323 **Acknowledgements**

324 This work was partly supported by The Great Britain Sasakawa Foundation [grant numbers 5029 (Bezodis) and 5226
325 (Willmott)] which had no involvement in the study design, study execution, the writing of the manuscript, or the
326 decision to submit it for publication. The authors thank Naoki Numazu for his assistance with data collection and
327 processing.

328

329 **Conflict of interest**

330 The authors declare no conflicts of interest to report in this research.

331

332 **References**

333 Apriantono, T., Nunome, H., Ikegami, Y., Sano, S., 2006. The effect of muscle fatigue on instep kicking kinetics and
334 kinematics in association football. *Journal of Sports Sciences*. 24, 951-960.

335 Atwater, A.E., 1979. Biomechanics of overarm throwing movements and of throwing injuries. *Exercise and Sport
336 Sciences Reviews* 7, 43-85.

337 Delp, S. L., Anderson, F. C., Arnold, A. S., Loan, P., Habib, A., John, C. T., Thelen, D. G., 2007. OpenSim:
338 open-source software to create and analyze dynamic simulations of movement. *IEEE Transactions on Biomedical
339 Engineering* 54, 1940-1950.

340 Dörge, H. C., Bullandersen, T, Sorensen, H., Simonsen, E. B. 2002. Biomechanical differences in soccer kicking with
341 the preferred and the non-preferred leg. *Journal of Sports Sciences*. 20, 293-299.

342 Elliott, B., Fleisig, G., Nicholls, R., Escamilla, R., 2003. Technique effects on upper limb loading in the tennis serve.
343 *Journal of Science and Medicine in Sport* 6, 76–87.

344 Feltner, M., Dapena, J., 1986. Dynamics of the shoulder and elbow joints of the throwing arm during a baseball pitch.
345 *International Journal of Sport Biomechanics* 2, 235-259.

346 Feltner, M.E., 1989. 3-dimensional interactions in a 2-segment kinetic chain. Part II: Application to the throwing arm
347 in baseball pitching. *International Journal of Sport Biomechanics* 5, 420–450.

348 Fleisig, G.S., Andrews, J.R., Dillman, C.J., Escamilla, R.F., 1995. Kinetics of baseball pitching with implications
349 about injury mechanisms. *American Journal of Sports Medicine* 23, 233-239.

350 Fleisig, G.S., Barrentine, S.W., Escamilla, R.F., Andrews, J.R., 1996a. Biomechanics of overhand throwing with
351 implications for injuries. *Sports Medicine* 21, 421-437.

352 Fleisig, G.S., Escamilla, R.F., Andrews, J.R., Matsuo, T., Satterwhite, Y., Barrentine, S.W., 1996b. Kinematic and
353 kinetic comparison between baseball pitching and football passing. *Journal of Applied Biomechanics* 12,
354 207-224.

355 Herring, R.M., Chapman, A.E., 1992. Effects of changes in segmental values and timing of both torque reversal in
356 simulated throws. *Journal of Biomechanics* 25, 1173-1184.

357 Hirashima, M., 2008. Induced acceleration analysis of three-dimensional multi-joint movements and its application to
358 sports movements. *Theoretical Biomechanics*, edited Vaclav Klika, InTech.

359 Hirashima, M., Kudo, K., Ohtsuki, T., 2007. A new non-orthogonal decomposition method to determine effective
360 torques for three-dimensional joint rotation. *Journal of Biomechanics* 40, 871-882.

361 Hirashima, M., Yamane, K., Nakamura, Y., Ohtsuki, T., 2008. Kinetic chain of overarm throwing in terms of joint
362 rotations revealed by induced acceleration analysis. *Journal of Biomechanics* 41, 2874-2883.

363 Kane, T. R., Levinson D. A., 1985. *Dynamics: Theory and Applications*. McGraw-Hill, New York, USA.

364 Kepple, T.M.; Siegel, K.L. Stanhope, S.J., 1997. Relative contributions of the lower extremity joint moments to
365 forward progression and support during gait. *Gait and Posture* 6, 1-8.

366 Kibler, W.B., 1995. Biomechanical analysis of the shoulder during tennis activities. *Clinics in Sports Medicine* 14,
367 79-85.

- 368 Kindall, J., 1992. Science of coaching baseball. Human Kinetics Publishers.
- 369 Koike, S., Bezodis, N., 2017. Determining the dynamic contributions to kicking foot speed in rugby place kicking. In
370 Proceedings of the 35th International Conference on Biomechanics in Sports, German Sport University Cologne,
371 Cologne.
- 372 Koike, S., Harada, Y., 2014. Dynamic Contribution Analysis of Tennis-serve-motion in Consideration of Torque
373 Generating Mode, *Procedia Engineering* 72, 97–102.
- 374 Koike, S., Mimura, K., 2016a. Contributions of joint torques, motion-dependent term and gravity to the generation of
375 baseball bat head speed. *Procedia Engineering* 147, 191-196.
- 376 Koike, S., Mimura, K., 2016b. Main contributors to the baseball bat head speed considering the generating factor of
377 motion-dependent term. *Procedia Engineering* 147, 197-202.
- 378 Koike, S., Nakaya, S., Mori, H., Ishikawa, T., Willmott, A.P., 2017. Modelling error distribution in the ground reaction
379 force during an induced-acceleration analysis of running in rear-foot strikers. *Journal of Sports Sciences*,
380 (Published online).
- 381 Koike, S., Uzawa, H., Hirayama, D., 2018. Generation mechanism of linear and angular ball velocity in baseball
382 pitching. *Proceedings* 2018, 2, 206.
- 383 Lees, A., Rahnama, N., 2013. Variability and typical error in the kinematics and kinetics of the maximal instep kick in
384 soccer. *Sports Biomechanics* 12, 283–292.
- 385 Naito, K., Fukui, Y., Maruyama, T., 2010. Multijoint kinetic chain analysis of knee extension during the soccer instep
386 kick. *Human Movement Science* 29, 259-276.
- 387 Naito, K., Maruyama, T., 2008. Contributions of the muscular torques and motion-dependent torques to generate rapid

388 elbow extension during overhand baseball pitching. *Sports Engineering* 11, 47-56.

389 Naito, K., Takagi, T., Kubota, H., Maruyama, T., 2017. Multi-body dynamic coupling mechanism for generating
390 throwing arm velocity during baseball pitching. *Human Movement Science* 54, 363-376.

391 Naito, K., Takagi, H., Yamada, N., Hashimoto, S., Maruyama, T., 2014. Intersegmental dynamics of 3D upper arm and
392 forearm longitudinal axis rotations during baseball pitching. *Human Movement Science* 38, 116-132.

393 Nunome, H., Asai, T., Ikegami, Y., Sakurai, S., 2002. Three-dimensional kinetic analysis of side-foot and instep soccer
394 kicks. *Medicine and Science in Sports and Exercise* 34, 2028-2036.

395 Peacock, J.C.A., Ball, K., 2017. The relationship between foot-ball impact and flight characteristics in punt kicking.
396 *Sports Engineering* 20, 221-230.

397 Putnam, C.A., 1991. A segment interaction analysis of proximal-to-distal sequential segment motion patterns.
398 *Medicine and Sciences in Sports and Exercise* 23, 130-144.

399 Putnam, C.A., 1993. Sequential motions of body segments in striking and throwing skills: Descriptions and
400 explanations. *Journal of Biomechanics* 26, 125-135.

401 Reid M., Elliott B., Alderson J., 2007. Shoulder joint loading in the high performance flat and kick tennis serves.
402 *British Journal of Sports Medicine* 41, 884–889.

403 Shinkai, H., Nunome, H., Isokawa, M., Ikegami, Y., 2009. Ball impact dynamics of instep soccer kicking. *Medicine*
404 *and Science in Sports and Exercise* 41, 889-897.

405 Zajac, F.E., Neptune, R.R., Kautz, S.A., 2002. Biomechanics and muscle coordination of human walking. Part I:
406 introduction to concepts, power, transfer, dynamics and simulations. *Gait and Posture* 16, 215-232.

407 Zajac, F.E., Neptune, R.R., Kautz, S.A., 2003. Biomechanics and muscle coordination of human walking. Part II:

408 lessons from dynamical simulations and clinical applications. *Gait and Posture* 17, 1-17.

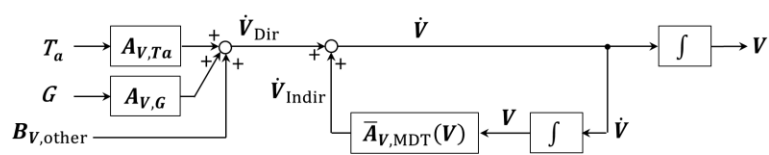
409 Zhang, Y., Liu, G., Xie, S., 2012. Movement sequences during instep rugby kick: a 3D biomechanical analysis.

410 *International Journal of Sports Science and Engineering*, 6, 89-95.

411

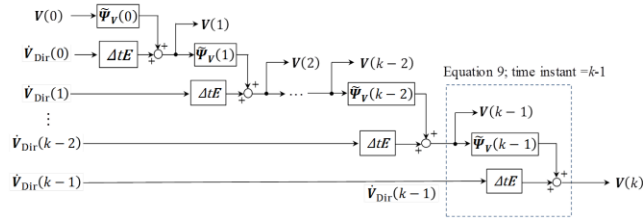
412

413 Figure 1. A block diagram representing the relationships between accelerations arising from the direct and indirect
 414 effects of inputs (e.g. joint torques, gravity and other terms) and the generalised acceleration and velocity vectors.
 415 Plain arrows indicate multiplication of the input vector with the matrix inside the box to which the arrow is pointing,
 416 with the exception of boxes including \int , which correspond to a time-integral operation.

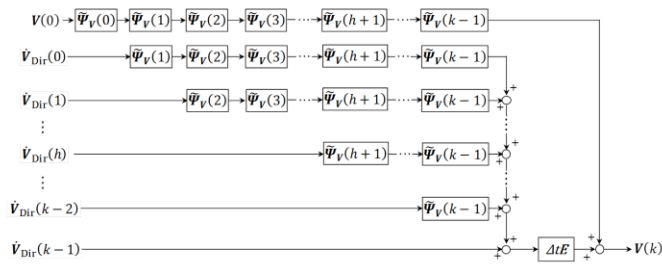


417
 418

419 Figure 2. A block diagram representing the recurrence formula with respect to the generalised velocity vector. Plain
 420 arrows correspond to multiplication of the input vector with the matrix inside the box to which the arrow is pointing.
 421 Reshaping Figure 2a into b identifies the contributions due to individual terms \dot{V}_{Dir} , as expressed in Equation 5, at
 422 each time instant to the generation of the generalized velocity vector including the motion-dependent processes of the
 423 torque inputs arising at any later time.



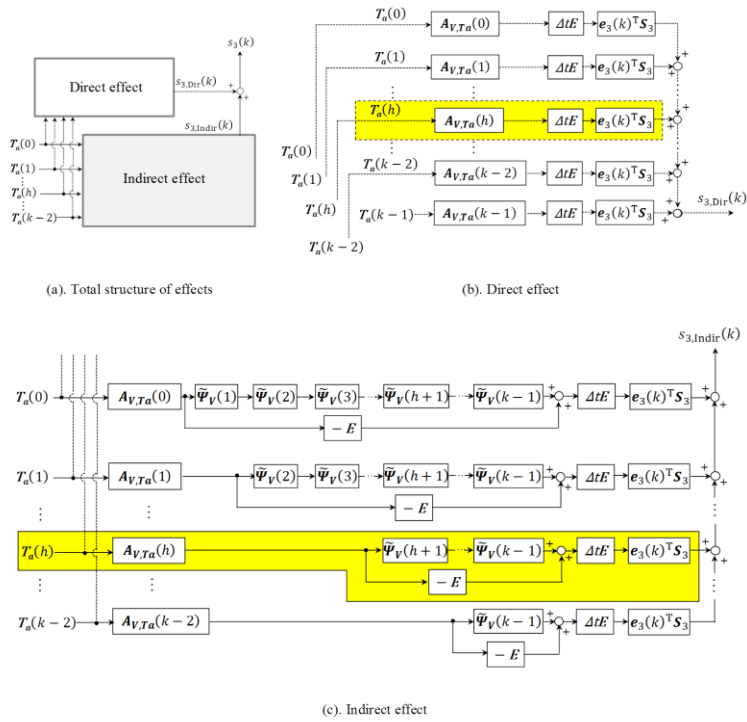
(a). A block diagram representing the recurrence formula with respect to the generalised velocity vector.



(b). A reshaped block diagram representing the recurrence formula with respect to the generalised velocity vector.

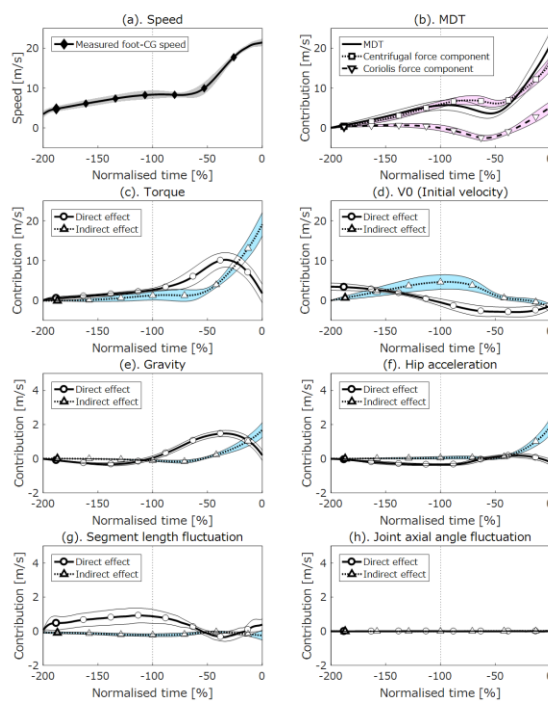
424
 425

426 Figure 3. A block diagram representing the direct and indirect effects of joint torque inputs to the generation of foot
 427 segment speed s_3 at time k . Plain arrows correspond to multiplication of the input vector with the matrix inside the box
 428 to which the arrow is pointing. The highlighted part of individual block diagrams in the direct effect (Figure 3b) and
 429 the indirect effect (Figure 3c) show respectively the contributions of the direct and indirect effects of joint torque
 430 inputs at time instant h to the generation of the foot CG's speed at BC.



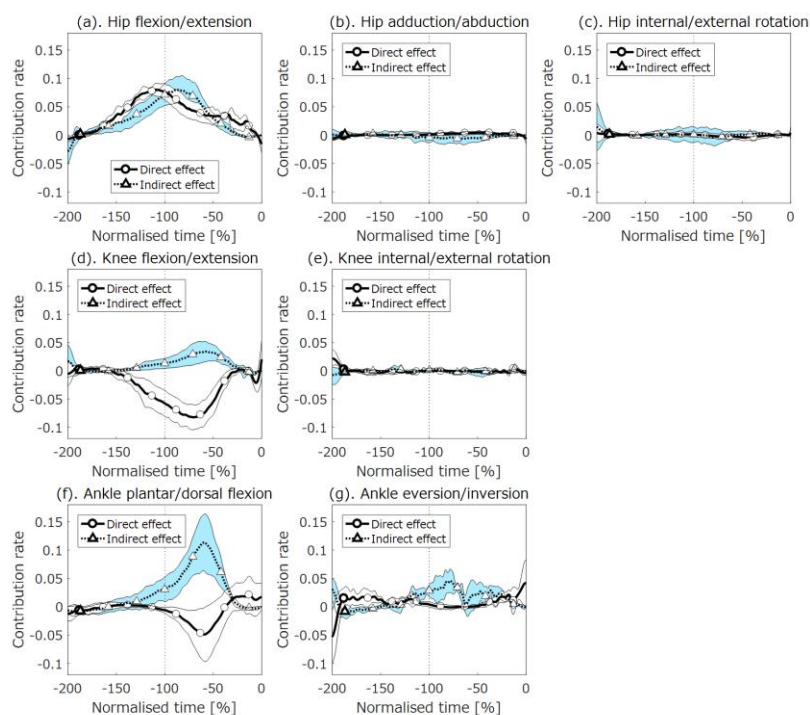
431
 432

433 Figure 4. Time-curve contributions of the direct and indirect effects of individual terms to the generation of the
 434 kicking foot CG's speed $s_3(k)$ for $k=-200\%$ to 0% (normalised) time. The values shown are the integrated
 435 contributions due to the direct and indirect effects of each source from $t=-200\%$ to k . Each line represents the mean
 436 across the participants at each normalised time, and the white-coloured and shaded regions indicate one standard
 437 deviation either side of the mean. Note: the scale in Figures e to h differs from the one in Figures a to d for visual
 438 purposes. For clarity, the contributions from gyroscopic effect moments and segment length fluctuations have been
 439 omitted from Figure b because the magnitudes of their mean values across the participants were less than 0.14 m/s and
 440 0.4 m/s, respectively, throughout.



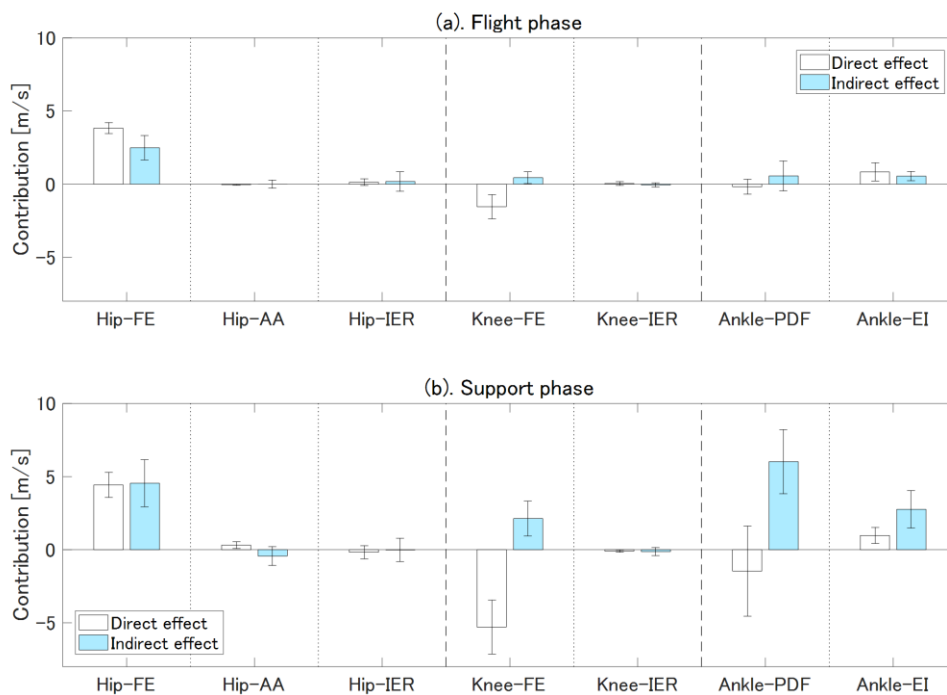
441
 442

443 Figure 5. Time-curve contribution rates of the direct and indirect effects of joint torque inputs at each instant during
 444 the flight and support phases to the generation of kicking-side foot CG's speed at ball contact $s_3(k_{BC})$. The units of
 445 the vertical axis for each graph are m/s per millisecond. These contribution rates indicate the time when, and the
 446 specific axis about which, each of the analysed torques induced the foot CG's speed at BC. The white-coloured and
 447 shaded regions indicate one standard deviation either side of the mean.



448
 449

450 Figure 6. Mean and standard deviation for the integrated contributions from the direct and indirect effects of joint
451 torque inputs during the flight and support phases to the generation of foot CG's speed at ball contact; these
452 correspond to the areas under the respective curves in Figure 5 (pre- and post-SFC, 100%).



453
454

Appendices

Appendix 1

Figure A1 shows a schematic diagram of a kicking-leg model containing three rigid segments – the thigh, shank and foot – with the lower trunk segment also described but not included in the model. Under the assumption that the human body can be modelled as a multi-linked system of rigid segments, the dynamical equations for individual segments can be expressed in a matrix form with respect to all segments as follows (Koike et al., 2017):

$$\mathbf{M}\dot{\mathbf{V}} = \mathbf{P}\mathbf{F} + \mathbf{Q}\mathbf{N} + \mathbf{H} + \mathbf{G} \quad (\text{A1})$$

where \mathbf{M} is the inertia matrix, and \mathbf{V} is the generalised velocity vector consisting of linear velocity vectors and angular velocity vectors for all the segments. \mathbf{P} is the coefficient matrix for vector \mathbf{F} which contains all joint force vectors. \mathbf{Q} is the coefficient matrix for vector \mathbf{N} which contains all joint moment vectors. \mathbf{H} is the gyroscopic effect moment vector, and \mathbf{G} is the vector due to the gravitational force.

Details of the matrices identified in the dynamical equations in Equation A1 are as follows: matrices \mathbf{O} and \mathbf{E} , without a subscript, denote the zero and unit matrices with three rows and three columns, and matrix \mathbf{O} with a subscript $m \times n$ denotes the zero matrix with m rows and n columns.

$$\mathbf{V} = [\dot{\mathbf{x}}_1^T \ \boldsymbol{\omega}_1^T \ \dot{\mathbf{x}}_2^T \ \boldsymbol{\omega}_2^T \ \dot{\mathbf{x}}_3^T \ \boldsymbol{\omega}_3^T]^T, \mathbf{F} = [\mathbf{f}_1^T \ \mathbf{f}_2^T \ \mathbf{f}_3^T]^T, \mathbf{N} = [\mathbf{n}_1^T \ \mathbf{n}_2^T \ \mathbf{n}_3^T]^T \quad (\text{A2})$$

$$\mathbf{M} = \text{block diag}\{m_1\mathbf{E}, \hat{\mathbf{I}}_1, m_2\mathbf{E}, \hat{\mathbf{I}}_2, m_3\mathbf{E}, \hat{\mathbf{I}}_3\} \quad (\text{A3})$$

$$\mathbf{P} = \begin{bmatrix} \mathbf{E} & -\mathbf{E} & \mathbf{0} \\ [\mathbf{r}_{1,\overline{\text{cg-P}}} \times] & -[\mathbf{r}_{1,\overline{\text{cg-D}}} \times] & \mathbf{0} \\ \mathbf{0} & \mathbf{E} & -\mathbf{E} \\ \mathbf{0} & [\mathbf{r}_{2,\overline{\text{cg-P}}} \times] & -[\mathbf{r}_{2,\overline{\text{cg-D}}} \times] \\ \mathbf{0} & \mathbf{0} & \mathbf{E} \\ \mathbf{0} & \mathbf{0} & [\mathbf{r}_{3,\overline{\text{cg-P}}} \times] \end{bmatrix}, \mathbf{Q} = \begin{bmatrix} \mathbf{0} & \mathbf{0} & \mathbf{0} \\ \mathbf{E} & -\mathbf{E} & \mathbf{0} \\ \mathbf{0} & \mathbf{0} & \mathbf{0} \\ \mathbf{0} & \mathbf{E} & -\mathbf{E} \\ \mathbf{0} & \mathbf{0} & \mathbf{0} \\ \mathbf{0} & \mathbf{0} & \mathbf{E} \end{bmatrix}, \mathbf{H} = \begin{bmatrix} \mathbf{0}_{3 \times 1} \\ -\boldsymbol{\omega}_1 \times (\hat{\mathbf{I}}_1 \boldsymbol{\omega}_1) \\ \mathbf{0}_{3 \times 1} \\ -\boldsymbol{\omega}_2 \times (\hat{\mathbf{I}}_2 \boldsymbol{\omega}_2) \\ \mathbf{0}_{3 \times 1} \\ -\boldsymbol{\omega}_3 \times (\hat{\mathbf{I}}_3 \boldsymbol{\omega}_3) \end{bmatrix}, \mathbf{G} = \begin{bmatrix} m_1 \mathbf{g} \\ \mathbf{0}_{3 \times 1} \\ m_2 \mathbf{g} \\ \mathbf{0}_{3 \times 1} \\ m_3 \mathbf{g} \\ \mathbf{0}_{3 \times 1} \end{bmatrix} \quad (\text{A4})$$

471

472

** Figure A1 near here **

473

474

Assuming that every segment is connected to its adjacent segment at a joint, the geometric constraint for linked

475

segments for all joints can be represented in matrix form as:

$$\mathbf{C}\dot{\mathbf{V}} + \dot{\mathbf{C}}\mathbf{V} = \dot{\boldsymbol{\eta}} + \mathbf{B}\ddot{\mathbf{x}}_{\text{Hip}} \quad (\text{A5})$$

476

where \mathbf{C} is the coefficient matrix for vector \mathbf{V} , and $\dot{\boldsymbol{\eta}}$ is the vector consisting of the differences between the distal and

477

proximal point velocity vectors at individual joints (Koike et al., 2017). The matrix \mathbf{B} is the coefficient matrix of hip

478

joint acceleration $\ddot{\mathbf{x}}_{\text{Hip}}$.

479

$$\mathbf{C} = \begin{bmatrix} -\mathbf{E} & [\mathbf{r}_{1,\overline{\text{cg-P}}} \times] & \mathbf{0} & \mathbf{0} & \mathbf{0} & \mathbf{0} \\ \mathbf{E} & -[\mathbf{r}_{1,\overline{\text{cg-D}}} \times] & -\mathbf{E} & [\mathbf{r}_{2,\overline{\text{cg-P}}} \times] & \mathbf{0} & \mathbf{0} \\ \mathbf{0} & \mathbf{0} & \mathbf{E} & -[\mathbf{r}_{2,\overline{\text{cg-D}}} \times] & -\mathbf{E} & [\mathbf{r}_{3,\overline{\text{cg-P}}} \times] \end{bmatrix}, \boldsymbol{\eta} = \begin{bmatrix} \ddot{\mathbf{r}}_{1,\overline{\text{cg-P}}}^* \\ \ddot{\mathbf{r}}_{2,\overline{\text{cg-P}}}^* - \ddot{\mathbf{r}}_{1,\overline{\text{cg-D}}}^* \\ \ddot{\mathbf{r}}_{3,\overline{\text{cg-P}}}^* - \ddot{\mathbf{r}}_{2,\overline{\text{cg-D}}}^* \end{bmatrix}, \mathbf{B} = \begin{bmatrix} -\mathbf{E} \\ \mathbf{0} \\ \mathbf{0} \end{bmatrix} \quad (\text{A6})$$

480

$$\dot{\mathbf{C}} = \begin{bmatrix} \mathbf{0} & [(\mathbf{2}\dot{\mathbf{r}}_{1,\overline{\text{cg-P}}}^* + \boldsymbol{\omega}_1 \times \mathbf{r}_{1,\overline{\text{cg-P}}}) \times] & \mathbf{0} & \mathbf{0} & \mathbf{0} & \mathbf{0} \\ \mathbf{0} & -[(\mathbf{2}\dot{\mathbf{r}}_{1,\overline{\text{cg-D}}}^* + \boldsymbol{\omega}_1 \times \mathbf{r}_{1,\overline{\text{cg-D}}}) \times] & \mathbf{0} & [(\mathbf{2}\dot{\mathbf{r}}_{2,\overline{\text{cg-P}}}^* + \boldsymbol{\omega}_2 \times \mathbf{r}_{2,\overline{\text{cg-P}}}) \times] & \mathbf{0} & \mathbf{0} \\ \mathbf{0} & \mathbf{0} & \mathbf{0} & -[(\mathbf{2}\dot{\mathbf{r}}_{2,\overline{\text{cg-D}}}^* + \boldsymbol{\omega}_2 \times \mathbf{r}_{2,\overline{\text{cg-D}}}) \times] & \mathbf{0} & [(\mathbf{2}\dot{\mathbf{r}}_{3,\overline{\text{cg-P}}}^* + \boldsymbol{\omega}_3 \times \mathbf{r}_{3,\overline{\text{cg-P}}}) \times] \end{bmatrix} \quad (\text{A7})$$

481

482

The equations for the anatomical constraint axes (e.g. varus/valgus axis at the knee joint), about which the joints

483

cannot rotate freely, can be characterised as follows (Koike et al., 2017):

$$\mathbf{A}\dot{\mathbf{V}} + \dot{\mathbf{A}}\mathbf{V} = \ddot{\boldsymbol{\varphi}} \quad (\text{A8})$$

484 where \mathbf{A} is the coefficient matrix for the vector \mathbf{V} , and $\ddot{\boldsymbol{\varphi}}$ is the vector consisting of double differentiated values of
 485 the two-set of inner products (i.e. $\mathbf{e}_{1,x}^T \mathbf{e}_{2,z} = \varphi_2$ at knee joint; $\mathbf{e}_{2,x}^T \mathbf{e}_{3,z} = \varphi_3$ at ankle joint) of unit vectors of
 486 adjacent segments, expressing anatomical constraints.

487 Details of the matrices identified in the anatomical constraint equations in Equation A8 are as follows:

$$\boldsymbol{\varphi} = \begin{bmatrix} \varphi_2(t) \\ \varphi_3(t) \end{bmatrix}, \mathbf{A} = \begin{bmatrix} \mathbf{0}_{1 \times 3} & -\mathbf{e}_{2,z}^T [\mathbf{e}_{1,x} \times] & \mathbf{0}_{1 \times 3} & -\mathbf{e}_{1,x}^T [\mathbf{e}_{2,z} \times] & \mathbf{0}_{1 \times 3} & \mathbf{0}_{1 \times 3} \\ \mathbf{0}_{1 \times 3} & \mathbf{0}_{1 \times 3} & \mathbf{0}_{1 \times 3} & -\mathbf{e}_{3,z}^T [\mathbf{e}_{2,x} \times] & \mathbf{0}_{1 \times 3} & -\mathbf{e}_{2,x}^T [\mathbf{e}_{3,z} \times] \end{bmatrix} \quad (\text{A9})$$

$$\dot{\mathbf{A}} = \begin{bmatrix} \mathbf{0}_{1 \times 3} & \dot{\mathbf{A}}_{1,2} & \mathbf{0}_{1 \times 3} & \dot{\mathbf{A}}_{1,4} & \mathbf{0}_{1 \times 3} & \mathbf{0}_{1 \times 3} \\ \mathbf{0}_{1 \times 3} & \mathbf{0}_{1 \times 3} & \mathbf{0}_{1 \times 3} & \dot{\mathbf{A}}_{2,4} & \mathbf{0}_{1 \times 3} & \dot{\mathbf{A}}_{2,6} \end{bmatrix}$$

$$\begin{cases} \dot{\mathbf{A}}_{1,2} = -(\boldsymbol{\omega}_2 \times \mathbf{e}_{2,z})^T [\mathbf{e}_{1,x} \times] - \mathbf{e}_{2,z}^T [(\boldsymbol{\omega}_1 \times \mathbf{e}_{1,x}) \times], \\ \dot{\mathbf{A}}_{1,4} = -(\boldsymbol{\omega}_1 \times \mathbf{e}_{1,x})^T [\mathbf{e}_{2,z} \times] - \mathbf{e}_{1,x}^T [(\boldsymbol{\omega}_2 \times \mathbf{e}_{2,z}) \times], \\ \dot{\mathbf{A}}_{2,4} = -(\boldsymbol{\omega}_3 \times \mathbf{e}_{3,z})^T [\mathbf{e}_{2,x} \times] - \mathbf{e}_{3,z}^T [(\boldsymbol{\omega}_2 \times \mathbf{e}_{2,x}) \times], \\ \dot{\mathbf{A}}_{2,6} = -(\boldsymbol{\omega}_2 \times \mathbf{e}_{2,x})^T [\mathbf{e}_{3,z} \times] - \mathbf{e}_{2,x}^T [(\boldsymbol{\omega}_3 \times \mathbf{e}_{3,z}) \times] \end{cases} \quad (\text{A10})$$

490
 491 The joint moment vector \mathbf{N} is considered to be the sum of an active joint torque vector \mathbf{T}_a and a constraint joint torque
 492 vector \mathbf{T}_p :

$$\mathbf{N} = \mathbf{S}_a \mathbf{T}_a + \mathbf{S}_p \mathbf{T}_p \quad (\text{A11})$$

493 where the matrices \mathbf{S}_a and \mathbf{S}_p are the coefficient matrices for \mathbf{T}_a and \mathbf{T}_p , respectively.

$$\mathbf{S}_a = \begin{bmatrix} \mathbf{K}_1^{-1} & \mathbf{0}_{3 \times 2} & \mathbf{0}_{3 \times 2} \\ \mathbf{0}_{3 \times 3} & \mathbf{K}_2^{-1} \begin{bmatrix} 1 & 0 & 0 \\ 0 & 0 & 1 \end{bmatrix}^T & \mathbf{0}_{3 \times 2} \\ \mathbf{0}_{3 \times 3} & \mathbf{0}_{3 \times 2} & \mathbf{K}_3^{-1} \begin{bmatrix} 1 & 0 & 0 \\ 0 & 0 & 1 \end{bmatrix}^T \end{bmatrix}, \mathbf{S}_p = \begin{bmatrix} \mathbf{0}_{3 \times 1} & \mathbf{0}_{3 \times 1} \\ \mathbf{K}_2^{-1} \begin{bmatrix} 0 & 1 & 0 \end{bmatrix}^T & \mathbf{0}_{3 \times 2} \\ \mathbf{0}_{3 \times 1} & \mathbf{K}_3^{-1} \begin{bmatrix} 0 & 1 & 0 \end{bmatrix}^T \end{bmatrix} \quad (\text{A12})$$

495

$$\begin{aligned} \mathbf{K}_1 &= [\mathbf{e}_{0,x} \quad \mathbf{e}'_{1,y} \quad \mathbf{e}_{1,z}], \quad \mathbf{e}'_{1,y} = (\mathbf{e}_{1,z} \times \mathbf{e}_{0,x}) / \|\mathbf{e}_{1,z} \times \mathbf{e}_{0,x}\| \\ \mathbf{K}_j &= [\mathbf{e}_{j-1,x} \quad \mathbf{e}_{j,y} \quad \mathbf{e}_{j,z}], \quad (j = 2, 3) \end{aligned} \quad (\text{A13})$$

496

497

where the unit vector $\mathbf{e}_{j,i}$ denotes the i -th axial vector of the j -th joint.

498

$$\mathbf{T}_a = [\tau_{1,x} \quad \tau_{1,y} \quad \tau_{1,z} \quad \tau_{2,x} \quad \tau_{2,z} \quad \tau_{3,x} \quad \tau_{3,z}]^T, \quad \mathbf{T}_p = [\tau_{2,y} \quad \tau_{3,y}]^T \quad (\text{A14})$$

499

500

The gyroscopic effect moment vector \mathbf{H} in Equation A1, which is also a function of the generalised velocity vector,

501

can be expressed in the form of the product of the coefficient matrix $\bar{\mathbf{H}}$ and the generalised velocity vector \mathbf{V} such

502

that:

$$\mathbf{H}(\mathbf{V}) = \bar{\mathbf{H}}(\mathbf{V})\mathbf{V} \quad (\text{A15})$$

503

Detail of the matrices identified in Equation A15 is as follows:

$$\bar{\mathbf{H}}(\mathbf{V}) = \text{block diag}\{\mathbf{O}, [(\hat{\mathbf{I}}_1 \boldsymbol{\omega}_1) \times], \mathbf{O}, [(\hat{\mathbf{I}}_2 \boldsymbol{\omega}_2) \times], \mathbf{O}, [(\hat{\mathbf{I}}_3 \boldsymbol{\omega}_3) \times]\} \quad (\text{A16})$$

504

Substituting Equations A5, A8 and A11 into Equation A1 yields a dynamic equation for the system as follows:

$$\begin{bmatrix} \dot{\mathbf{V}} \\ \mathbf{F} \\ \mathbf{T}_p \end{bmatrix} = \begin{bmatrix} \mathbf{M} & -\mathbf{P} & -\mathbf{Q}\mathbf{S}_p \\ \mathbf{C} & \mathbf{O}_{9 \times 9} & \mathbf{O}_{9 \times 2} \\ \mathbf{A} & \mathbf{O}_{2 \times 9} & \mathbf{O}_{2 \times 2} \end{bmatrix}^{-1} \left\{ \begin{bmatrix} \mathbf{Q}\mathbf{S}_p \\ \mathbf{O}_{9 \times 7} \\ \mathbf{O}_{2 \times 7} \end{bmatrix} \mathbf{T}_a + \begin{bmatrix} \bar{\mathbf{H}} \\ -\hat{\mathbf{C}} \\ -\hat{\mathbf{A}} \end{bmatrix} \mathbf{V} + \begin{bmatrix} \mathbf{E}_{18} \\ \mathbf{O}_{9 \times 18} \\ \mathbf{O}_{2 \times 18} \end{bmatrix} \mathbf{G} + \begin{bmatrix} \mathbf{O}_{18 \times 3} \\ \mathbf{B} \\ \mathbf{O}_{2 \times 3} \end{bmatrix} \ddot{\mathbf{x}}_{\text{Hip}} + \begin{bmatrix} \mathbf{O}_{18 \times 9} \\ \mathbf{E}_9 \\ \mathbf{O}_{2 \times 9} \end{bmatrix} \ddot{\boldsymbol{\eta}} + \begin{bmatrix} \mathbf{O}_{18 \times 2} \\ \mathbf{O}_{9 \times 2} \\ \mathbf{E}_2 \end{bmatrix} \ddot{\boldsymbol{\phi}} \right\} \quad (\text{A17})$$

505

where the matrices \mathbf{E}_n and $\mathbf{O}_{m \times n}$ denote a unit matrix with n rows and columns, and the zero matrix with m rows and n

506

columns, respectively.

507

Details of the matrices identified in the dynamical equations in Equations 2 and 3 are as follows.

$$\left. \begin{aligned}
A_{V,Ta} &= M^{-1}WQ_a, \\
\bar{A}_{V,M\Delta T} &= M^{-1}W\bar{H} + M^{-1}\{P\bar{H}_{FV} - Q_p(\Gamma Q_p)^{-1}\bar{H}_{TV}\}, \\
A_{V,G} &= M^{-1}W, \\
A_{V,Hip} &= M^{-1}\{P\bar{H}_{F\eta} - Q_p(\Gamma Q_p)^{-1}\bar{H}_{T\eta}\}B, \\
A_{V,\eta} &= M^{-1}\{P\bar{H}_{F\eta} - Q_p(\Gamma Q_p)^{-1}\bar{H}_{T\eta}\}, \\
A_{V,\phi} &= M^{-1}\{P\bar{H}_{F\phi} - Q_p(\Gamma Q_p)^{-1}\}
\end{aligned} \right\} \quad (A18)$$

508 where the temporary matrices W , Φ , Q_a , Q_b , \bar{H}_{FV} , Γ , \bar{H}_{TV} , $\bar{H}_{F\eta}$, $\bar{H}_{T\eta}$, $\bar{H}_{F\phi}$ and B are shown as follows:

$$\left. \begin{aligned}
W &= P\Phi - Q_p(\Gamma Q_p)^{-1}\Gamma + E, \\
\Phi &= (CM^{-1}P)^{-1}CM^{-1}\{Q_p(\Gamma Q_p)^{-1}\Gamma - E\}, \\
Q_a &= QS_a, \\
Q_p &= QS_p, \\
\bar{H}_{FV} &= (CM^{-1}P)^{-1}\{CM^{-1}Q_p(\Gamma Q_p)^{-1}\bar{H}_{TV} - \dot{C}\}, \\
\Gamma &= AM^{-1}\{E - P(CM^{-1}P)^{-1}CM^{-1}\}, \\
\bar{H}_{TV} &= \dot{A} - AM^{-1}P(CM^{-1}P)^{-1}\dot{C}, \\
\bar{H}_{F\eta} &= (CM^{-1}P)^{-1}\{CM^{-1}Q_p(\Gamma Q_p)^{-1}\bar{H}_{T\eta} + E\}, \\
\bar{H}_{T\eta} &= AM^{-1}P(CM^{-1}P)^{-1}, \\
\bar{H}_{F\phi} &= (CM^{-1}P)^{-1}CM^{-1}Q_p(\Gamma Q_p)^{-1}, \\
B &= [E_3 \quad O_{3 \times 3} \quad O_{3 \times 3}]^T
\end{aligned} \right\} \quad (A19)$$

509

510

Appendix 2

511 The contribution of each term at every instant to the generation of the generalised velocity vector can be derived from

512 Figure 2b which represents Equation 9. For example, the generalised velocity vector at time k can be calculated from

513 the time history of the input vector $\dot{V}_{Dir}(k)$ as follows:

$$V(k) = \Delta t \dot{V}_{Dir}(k-1) + \Delta t \sum_{h=1}^{k-1} \left[\left\{ \prod_{j=h}^{k-1} \tilde{\Psi}_V(j) \right\} \dot{V}_{Dir}(h-1) \right] + \left\{ \prod_{j=0}^{k-1} \tilde{\Psi}_V(j) \right\} V(0) \quad (A20)$$

514 where the function Π denotes the factorial function shown as

$$\prod_{j=h}^k \tilde{\Psi}_V(j) = \tilde{\Psi}_V(k)\tilde{\Psi}_V(k-1)\tilde{\Psi}_V(k-2)\dots\tilde{\Psi}_V(h) \quad (A21)$$

515 The generalised velocity vector at time k can be obtained from Equations A20 and A21 as the sums of individual
 516 contributions as follows:

$$\mathbf{V}(k) = \mathbf{C}_{V,Ta}(k) + \mathbf{C}_{V,G}(k) + \mathbf{C}_{V,V_0}(k) + \mathbf{C}_{V,other}(k),$$

$$\begin{cases} \mathbf{C}_{V,Ta}(k) = \Delta t \mathbf{A}_{V,Ta}(k-1) \mathbf{T}_a(k-1) + \Delta t \sum_{h=1}^{k-1} \left[\left\{ \prod_{j=h}^{k-1} \tilde{\Psi}_V(j) \right\} \mathbf{A}_{V,Ta}(h-1) \mathbf{T}_a(h-1) \right], \\ \mathbf{C}_{V,G}(k) = \Delta t \mathbf{A}_{V,G}(k-1) \mathbf{G} + \Delta t \sum_{h=0}^{k-1} \left[\left\{ \prod_{j=h}^{k-1} \tilde{\Psi}_V(j) \right\} \mathbf{A}_{V,G}(h-1) \mathbf{G} \right], \\ \mathbf{C}_{V,V_0}(k) = \left\{ \prod_{j=0}^{k-1} \tilde{\Psi}_V(j) \right\} \mathbf{V}(0) \end{cases} \quad (\text{A22})$$

517 where the vectors $\mathbf{C}_{V,Ta}$, $\mathbf{C}_{V,G}$, \mathbf{C}_{V,V_0} and $\mathbf{C}_{V,other}$ respectively denote total contributions of the active joint torque,
 518 gravity, the initial velocity term, and other terms (as expressed in Equation A23) to the generation of the generalised
 519 velocity vector $\mathbf{V}(k)$ in consideration of the generating factors of the MDT.

520 The vectors $\mathbf{C}_{V,Hip}$, $\mathbf{C}_{V,\eta}$ and $\mathbf{C}_{V,\varphi}$ denote total contributions of the hip-joint acceleration term, segment length
 521 fluctuation term, and constraint joint axial angle fluctuation term, respectively.

$$\mathbf{C}_{V,other}(k) = \mathbf{C}_{V,Hip}(k) + \mathbf{C}_{V,\eta}(k) + \mathbf{C}_{V,\varphi}(k),$$

$$\begin{cases} \mathbf{C}_{V,Hip}(k) = \Delta t \mathbf{A}_{V,Hip}(k-1) \ddot{\mathbf{x}}_{Hip}(k-1) + \Delta t \sum_{h=1}^{k-1} \left[\left\{ \prod_{j=h}^{k-1} \tilde{\Psi}_V(j) \right\} \mathbf{A}_{V,Hip}(h-1) \ddot{\mathbf{x}}_{Hip}(h-1) \right], \\ \mathbf{C}_{V,\eta}(k) = \Delta t \mathbf{A}_{V,\eta}(k-1) \ddot{\boldsymbol{\eta}}(k-1) + \Delta t \sum_{h=1}^{k-1} \left[\left\{ \prod_{j=h}^{k-1} \tilde{\Psi}_V(j) \right\} \mathbf{A}_{V,\eta}(h-1) \ddot{\boldsymbol{\eta}}(h-1) \right], \\ \mathbf{C}_{V,\varphi}(k) = \Delta t \mathbf{A}_{V,\varphi}(k-1) \ddot{\boldsymbol{\varphi}}(k-1) + \Delta t \sum_{h=1}^{k-1} \left[\left\{ \prod_{j=h}^{k-1} \tilde{\Psi}_V(j) \right\} \mathbf{A}_{V,\varphi}(h-1) \ddot{\boldsymbol{\varphi}}(h-1) \right] \end{cases} \quad (\text{A23})$$

522
 523 The generalised velocity vector at time k can be obtained from Equations 4, 5 and 7 as the sums of individual
 524 contributions as follows:

$$\mathbf{V}(k) = \mathbf{C}_{\text{Dir},V,T_a}(k) + \mathbf{C}_{\text{Dir},V,\text{MDT}}(k) + \mathbf{C}_{\text{Dir},V,G}(k) + \mathbf{C}_{\text{Dir},V,\text{other}}(k) + \mathbf{V}(0),$$

$$\begin{cases} \mathbf{C}_{\text{Dir},V,T_a}(k) = \Delta t \sum_{h=0}^{k-1} \mathbf{A}_{V,T_a}(h) \mathbf{T}_a(h), & \mathbf{C}_{\text{Dir},V,\text{MDT}}(k) = \Delta t \sum_{h=0}^{k-1} \bar{\mathbf{A}}_{V,\text{MDT}}(\mathbf{V}(h)) \mathbf{V}(h), \\ \mathbf{C}_{\text{Dir},V,G}(k) = \Delta t \sum_{h=0}^{k-1} \mathbf{A}_{V,G}(h) \mathbf{G}, & \mathbf{C}_{\text{Dir},V,\text{other}}(k) = \Delta t \sum_{h=0}^{k-1} \mathbf{A}_{V,\text{other}}(h) \end{cases} \quad (\text{A24})$$

525 where the contribution vectors $\mathbf{C}_{\text{Dir},V,T_a}$, $\mathbf{C}_{\text{Dir},V,\text{MDT}}$, $\mathbf{C}_{\text{Dir},V,G}$ and $\mathbf{C}_{\text{Dir},V,\text{other}}$ respectively denote direct effects of the active
526 joint torque, the motion-dependent term, the gravitational term, and other terms to the generation of the generalised
527 velocity vector $\mathbf{V}(k)$.

528 Furthermore, the direct effect of active joint torque input can be distributed into the sums of the direct effects of the
529 individual joint torque inputs as:

$$\mathbf{C}_{\text{Dir},V,T_a}(k) = \sum_{j_{\text{Axis}}=1}^{n_{\text{Axis}}} \mathbf{C}_{\text{Dir},V,T_a,j_{\text{Axis}}}(k),$$

$$\mathbf{C}_{\text{Dir},V,T_a,j_{\text{Axis}}}(k) = \Delta t \sum_{h=0}^{k-1} \mathbf{A}_{V,T_a,j_{\text{Axis}}}(h) \mathbf{T}_{a,j_{\text{Axis}}}(h)$$
(A25)

530 where n_{Axis} denotes the number of the active joint axes.

531

532 The total contribution is the sum of the direct and indirect effects of joint torque inputs:

$$\mathbf{C}_{V,T_a}(k) = \mathbf{C}_{\text{Dir},V,T_a}(k) + \mathbf{C}_{\text{Indir},V,T_a}(k)$$
(A26)

533

534 The indirect effect of the joint torque inputs is obtained from the difference between the total contribution and the
535 direct effect of joint torque inputs from Equation A26 as:

$$\mathbf{C}_{\text{Indir},V,T_a}(k) = \mathbf{C}_{V,T_a}(k) - \mathbf{C}_{\text{Dir},V,T_a}(k)$$
(A27)

536

537 ***Contributions to the kicking foot CG's speed***

538 As described in Equation A2, the linear velocity vector of the CG of the kicking foot $\dot{\mathbf{x}}_3(k)$ can be expressed as
 539 follows:

540

$$\dot{\mathbf{x}}_3(k) = \mathbf{S}_3 \mathbf{V}(k), \quad \mathbf{S}_3 = [\mathbf{0}_{3 \times 12} \quad \mathbf{E} \quad \mathbf{0}_{3 \times 3}] \quad (\text{A28})$$

541 where the matrix $\mathbf{S}_3(k)$ indicates the selective matrix which extracts the components of the linear velocity vector
 542 regarding the foot segment from the generalised velocity vector.

543 The unit vector, expressing the direction of the foot CG's velocity vector, is obtained by dividing the velocity vector
 544 by its magnitude as:

$$\mathbf{e}_3(k) = \frac{\dot{\mathbf{x}}_3(k)}{|\dot{\mathbf{x}}_3(k)|} \quad (\text{A29})$$

545

546 Finally, operating the inner product of Equation A29 with Equations A24 through A28 yields the dynamic
 547 contributions of individual terms to the generation of the point's speed at time k , $s_3(k)$, shown as:

$$s_3(k) = C_{s3, Ta}(k) + C_{s3, G}(k) + C_{s3, other}(k) + C_{s3, V_0}(k) \quad (\text{A30})$$

548 where the terms $C_{s3, Ta}(k)$, $C_{s3, G}(k)$ and $C_{s3, other}(k)$ respectively denote the contributions of the joint torque term,
 549 gravitational term and other terms to the foot CG's speed. The term $C_{s3, V_0}(k)$ denotes the contribution of the initial
 550 velocity term, i.e. the velocity of the system at the start of the analysis.

551 For example, the contribution of the active joint torque to the generation of the foot CG's speed at time k is expressed
 552 as follows:

$$C_{s3,Ta}(k) = \mathbf{e}_3^T(k) \bar{\mathbf{S}}_3 \left(\Delta t \mathbf{A}_{V,Ta}(k-1) \mathbf{T}_a(k-1) + \Delta t \sum_{h=1}^{k-1} \left[\left\{ \prod_{j=h}^{k-1} \tilde{\Psi}_V(j) \right\} \mathbf{A}_{V,Ta}(h-1) \mathbf{T}_a(h-1) \right] \right) \quad (\text{A31})$$

553

$$C_{\text{Dir},s3,Ta}(k) = \mathbf{e}_3^T(k) \bar{\mathbf{S}}_3 \Delta t \sum_{h=0}^{k-1} \mathbf{A}_{V,Ta}(h) \mathbf{T}_a(h), \quad (\text{A32})$$

554

$$\begin{aligned} C_{\text{Indir},s3,Ta}(k) &= C_{s3,Ta}(k) - C_{\text{Dir},s3,Ta}(k) \\ &= \mathbf{e}_3^T(k) \bar{\mathbf{S}}_3 \Delta t \sum_{h=1}^{k-1} \left(\left\{ \prod_{j=h}^{k-1} \tilde{\Psi}_V(j) \right\} - \mathbf{E}_{18} \right) \mathbf{A}_{V,Ta}(h-1) \mathbf{T}_a(h-1) \end{aligned} \quad (\text{A33})$$

555

According to Equations A31 and A32, the direct and indirect effects of a joint torque inputted at time h (any given

556

instant in time between swing start and time k), $C_{\text{Inst},s3,BC,Ta}(h)$ and $C_{\text{Cumul},s3,BC,Ta}(h)$ to the generation of the foot CG's

557

speed at BC are expressed as follows:

$$C_{\text{Dir},s3,BC,Ta}(h) = \mathbf{e}_3^T(k_{\text{BC}}) \bar{\mathbf{S}}_3 \Delta t \mathbf{A}_{V,Ta}(h) \mathbf{T}_a(h), \quad (\text{A34})$$

558

$$C_{\text{Indir},s3,BC,Ta}(h) = \mathbf{e}_3^T(k_{\text{BC}}) \bar{\mathbf{S}}_3 \Delta t \left(\left\{ \prod_{j=h+1}^{k_{\text{BC}}-1} \tilde{\Psi}_V(j) \right\} - \mathbf{E}_{18} \right) \mathbf{A}_{V,Ta}(h) \mathbf{T}_a(h) \quad (\text{A35})$$

559

The individual contributions of the active joint torques, expressed by Equations A31 through A35, can be furthermore

560

divided into the contributions of the individual active joint torques about each individual axis of a joint (not shown).

561

562

Appendix 3

563

Decomposition of the MDT into kinematic components

564

The contribution of the MDT to the generalised acceleration vector can be expressed in the following form when using

565 Equation A17:

$$\mathbf{C}_{\dot{V},\text{MDT}} = \bar{\mathbf{A}}_{V,\text{MDT}}(\mathbf{V})\mathbf{V} = \mathbf{S}_{\dot{V}}\mathbf{B}_{\text{sys}} \begin{bmatrix} \bar{\mathbf{H}} \\ -\dot{\mathbf{C}} \\ -\dot{\mathbf{A}} \end{bmatrix} \mathbf{V}, \quad (\text{A36})$$

$$\mathbf{S}_{\dot{V}} = [\mathbf{E}_{18} \quad \mathbf{O}_{18 \times 9} \quad \mathbf{O}_{18 \times 2}], \quad \mathbf{B}_{\text{sys}} = \begin{bmatrix} \mathbf{M} & -\mathbf{P} & -\mathbf{Q}\mathbf{S}_p \\ \mathbf{C} & \mathbf{O}_{9 \times 9} & \mathbf{O}_{9 \times 2} \\ \mathbf{A} & \mathbf{O}_{2 \times 9} & \mathbf{O}_{2 \times 2} \end{bmatrix}^{-1}$$

566 where matrix $\mathbf{S}_{\dot{V}}$ denotes the selective matrix extracting the generalised acceleration components from Equation A17,

567 and matrix \mathbf{B}_{sys} indicates the coefficient matrix of the target system shown in Equation A17. This equation can be

568 expressed as the sum of three terms, as shown in the following equation:

$$\mathbf{C}_{\dot{V},\text{MDT}} = \mathbf{S}_{\dot{V}}\mathbf{B}_{\text{sys}} \begin{bmatrix} \bar{\mathbf{H}}\mathbf{V} \\ \mathbf{O}_{9 \times 1} \\ \mathbf{O}_{2 \times 1} \end{bmatrix} - \mathbf{S}_{\dot{V}}\mathbf{B}_{\text{sys}} \begin{bmatrix} \mathbf{O}_{18 \times 1} \\ \dot{\mathbf{C}}_B\mathbf{V} \\ \mathbf{O}_{2 \times 1} \end{bmatrix} - \mathbf{S}_{\dot{V}}\mathbf{B}_{\text{sys}} \begin{bmatrix} \mathbf{O}_{18 \times 1} \\ \dot{\mathbf{C}}_C\mathbf{V} \\ \dot{\mathbf{A}}\mathbf{V} \end{bmatrix}, \quad (\text{A37})$$

$$\left\{ \begin{array}{l} \dot{\mathbf{C}}_B = \begin{bmatrix} \mathbf{O} & [2\dot{\mathbf{r}}_{1,\text{cg-P}}^* \times] & \mathbf{O} & \mathbf{O} & \mathbf{O} & \mathbf{O} \\ \mathbf{O} & -[2\dot{\mathbf{r}}_{1,\text{cg-D}}^* \times] & \mathbf{O} & [2\dot{\mathbf{r}}_{2,\text{cg-P}}^* \times] & \mathbf{O} & \mathbf{O} \\ \mathbf{O} & \mathbf{O} & \mathbf{O} & -[2\dot{\mathbf{r}}_{2,\text{cg-D}}^* \times] & \mathbf{O} & [2\dot{\mathbf{r}}_{3,\text{cg-P}}^* \times] \end{bmatrix}, \\ \dot{\mathbf{C}}_C = \begin{bmatrix} \mathbf{O} & [(\boldsymbol{\omega}_1 \times \mathbf{r}_{1,\text{cg-P}}) \times] & \mathbf{O} & \mathbf{O} & \mathbf{O} & \mathbf{O} \\ \mathbf{O} & -[(\boldsymbol{\omega}_1 \times \mathbf{r}_{1,\text{cg-D}}) \times] & \mathbf{O} & [(\boldsymbol{\omega}_2 \times \mathbf{r}_{2,\text{cg-P}}) \times] & \mathbf{O} & \mathbf{O} \\ \mathbf{O} & \mathbf{O} & \mathbf{O} & -[(\boldsymbol{\omega}_2 \times \mathbf{r}_{2,\text{cg-D}}) \times] & \mathbf{O} & [(\boldsymbol{\omega}_3 \times \mathbf{r}_{3,\text{cg-P}}) \times] \end{bmatrix} \end{array} \right.$$

569 where the terms on the right side of this equation represent, in turn, the gyroscopic effect moment component, the

570 segment length fluctuation component, and the centrifugal and Coriolis forces component of the contribution of the

571 MDT to the generalised acceleration vector. Matrices $\dot{\mathbf{C}}_B$ and $\dot{\mathbf{C}}_C$ denote the coefficient matrices with respect to the

572 generalised velocity vector and their sum is equal to $\dot{\mathbf{C}}$ in Equation A7.

573

574 The angular velocity vector of the i -th segment is expressed as the sum of $\boldsymbol{\omega}_0$ and the summation of the products of

575 multiplying the joint angular velocity $\dot{\theta}_{i_c,l_c}$ by the unit vector of the joint axial vector \mathbf{e}_{i_c,l_c} as:

$$\boldsymbol{\omega}_i = \boldsymbol{\omega}_0 + \sum_{i_c=1}^i \sum_{l_c=1}^{n(i_c)} \dot{\theta}_{i_c,l_c} \mathbf{e}_{i_c,l_c}, \quad n = [3, 2, 2], \quad i = 1, 2, 3 \quad (\text{A38})$$

$$\begin{cases} \mathbf{e}_{1,1} = \mathbf{e}_{0,x}, & \mathbf{e}_{1,2} = \mathbf{e}'_{1,y}, & \mathbf{e}_{1,3} = \mathbf{e}_{1,z}, \\ \mathbf{e}_{2,1} = \mathbf{e}_{1,x}, & \mathbf{e}_{2,2} = \mathbf{e}_{2,z}, \\ \mathbf{e}_{3,1} = \mathbf{e}_{2,x}, & \mathbf{e}_{3,2} = \mathbf{e}_{3,z} \end{cases}$$

576 where the vector $\mathbf{e}'_{1,y}$ is the unit vector defined in Equation A13, and i_c and l_c are dummy variables used in the
577 summation.

578 The components of the vector $\dot{\mathbf{A}}\mathbf{V}$, which is in the third term of the right-side of Equation A37, are expressed by the
579 following equation from Equation A10:

$$\dot{\mathbf{A}}\mathbf{V} = \begin{bmatrix} -2(\boldsymbol{\omega}_2 \times \mathbf{e}_{2,z})^T (\mathbf{e}_{1,x} \times \boldsymbol{\omega}_1) - \mathbf{e}_{2,z}^T [(\boldsymbol{\omega}_1 \times \mathbf{e}_{1,x}) \times \boldsymbol{\omega}_1] - \mathbf{e}_{1,x}^T [(\boldsymbol{\omega}_2 \times \mathbf{e}_{2,z}) \times \boldsymbol{\omega}_2] \\ -2(\boldsymbol{\omega}_3 \times \mathbf{e}_{3,z})^T (\mathbf{e}_{2,x} \times \boldsymbol{\omega}_2) - \mathbf{e}_{3,z}^T [(\boldsymbol{\omega}_2 \times \mathbf{e}_{2,x}) \times \boldsymbol{\omega}_2] - \mathbf{e}_{2,x}^T [(\boldsymbol{\omega}_3 \times \mathbf{e}_{3,z}) \times \boldsymbol{\omega}_3] \end{bmatrix} \quad (\text{A39})$$

580 The components of the vector $\dot{\mathbf{C}}_c\mathbf{V}$ are expressed by the following equation:

$$\dot{\mathbf{C}}_c\mathbf{V} = \begin{bmatrix} (\boldsymbol{\omega}_1 \times \mathbf{r}_{1,\overline{\text{cg-P}}}) \times \boldsymbol{\omega}_1 \\ -(\boldsymbol{\omega}_1 \times \mathbf{r}_{1,\overline{\text{cg-D}}}) \times \boldsymbol{\omega}_1 + (\boldsymbol{\omega}_2 \times \mathbf{r}_{2,\overline{\text{cg-P}}}) \times \boldsymbol{\omega}_2 \\ -(\boldsymbol{\omega}_2 \times \mathbf{r}_{2,\overline{\text{cg-D}}}) \times \boldsymbol{\omega}_2 + (\boldsymbol{\omega}_3 \times \mathbf{r}_{3,\overline{\text{cg-P}}}) \times \boldsymbol{\omega}_3 \end{bmatrix} \quad (\text{A40})$$

581

582 When considering the angular velocity vector of the i -th segment as given in Equation A38, any element expressed as

583 $(\boldsymbol{\omega}_i \times \mathbf{r}_{i,s}) \times \boldsymbol{\omega}_i$ can be divided into five components that arise from either centrifugal forces or Coriolis forces:

$$\begin{aligned} (\boldsymbol{\omega}_i \times \mathbf{r}_{i,s}) \times \boldsymbol{\omega}_i &= (\boldsymbol{\omega}_0 \times \mathbf{r}_{i,s}) \times \boldsymbol{\omega}_0 && : \text{Centrifugal force term} \\ &+ \sum_{i_c=1}^i \sum_{l_c=1}^{n(i_c)} \dot{\theta}_{i_c,l_c}^2 (\mathbf{e}_{i_c,l_c} \times \mathbf{r}_{i,s}) \times \mathbf{e}_{i_c,l_c} && : \text{Centrifugal force term} \\ &+ \left\{ \left(\sum_{i_c=1}^i \sum_{l_c=1}^{n(i_c)} \dot{\theta}_{i_c,l_c} \mathbf{e}_{i_c,l_c} \right) \times \mathbf{r}_{i,s} \right\} \times \boldsymbol{\omega}_0 && : \text{Coriolis force term} \\ &+ (\boldsymbol{\omega}_0 \times \mathbf{r}_{i,s}) \times \left(\sum_{i_c=1}^i \sum_{l_c=1}^{n(i_c)} \dot{\theta}_{i_c,l_c} \mathbf{e}_{i_c,l_c} \right) && : \text{Coriolis force term} \\ &+ \sum_{j_c=1}^j \sum_{h_c=1}^{n(j_c)} \sum_{i_c=1}^i \sum_{l_c=1}^{n(i_c)} \{ \alpha_{j_c,h_c,i_c,l_c} \dot{\theta}_{i_c,l_c} \dot{\theta}_{j_c,h_c} (\mathbf{e}_{i_c,l_c} \times \mathbf{r}_{i,s}) \times \mathbf{e}_{j_c,h_c} \}, && : \text{Coriolis force term} \\ &n = [3, 2, 2] \end{aligned} \quad (\text{A41})$$

584 where j_c and h_c are additional dummy variables used in the summations, and the coefficient in the fifth term in the
585 right side of Equation A41 α_{j_c,h_c,i_c,l_c} is given as:

$$\alpha_{j_c, h_c, i_c, l_c} = \begin{cases} 0 & \text{if } j_c = i_c \text{ and } h_c = l_c \\ 1 & \text{else} \end{cases} \quad (\text{A42})$$

586 and the subscript s of the position vector $\mathbf{r}_{i,s}$ denotes $\overline{\text{cg}-\text{D}}$ or $\overline{\text{cg}-\text{P}}$.

587 Any element expressed as $(\boldsymbol{\omega}_i \times \mathbf{e}_{i,z})^T (\mathbf{e}_{j,x} \times \boldsymbol{\omega}_j)$ in Equation A39 can be divided into five components
588 representing either centrifugal force terms or Coriolis force terms:

$$\begin{aligned} (\boldsymbol{\omega}_i \times \mathbf{e}_{i,z})^T (\mathbf{e}_{j,x} \times \boldsymbol{\omega}_j) = & (\boldsymbol{\omega}_0 \times \mathbf{e}_{i,z})^T (\mathbf{e}_{j,x} \times \boldsymbol{\omega}_0) && : \text{Centrifugal force term} \\ & + \sum_{j_c=1}^j \sum_{h_c=1}^{n(j_c)} \dot{\theta}_{j_c, h_c}^2 (\mathbf{e}_{j_c, h_c} \times \mathbf{e}_{i,z})^T (\mathbf{e}_{j,x} \times \mathbf{e}_{j_c, h_c}) && : \text{Centrifugal force term} \\ & + (\boldsymbol{\omega}_0 \times \mathbf{e}_{i,z})^T \left\{ \mathbf{e}_{j,x} \times \left(\sum_{j_c=1}^j \sum_{h_c=1}^{n(j_c)} \dot{\theta}_{j_c, h_c} \mathbf{e}_{j_c, h_c} \right) \right\} && : \text{Coriolis force term} \\ & + (\boldsymbol{\omega}_0 \times \mathbf{e}_{j,x})^T \left\{ \mathbf{e}_{i,z} \times \left(\sum_{i_c=1}^i \sum_{l_c=1}^{n(i_c)} \dot{\theta}_{i_c, l_c} \mathbf{e}_{i_c, l_c} \right) \right\} && : \text{Coriolis force term} \\ & + \sum_{j_c=1}^j \sum_{h_c=1}^{n(j_c)} \sum_{i_c=1}^i \sum_{l_c=1}^{n(i_c)} \left\{ \alpha_{j_c, h_c, i_c, l_c} \dot{\theta}_{i_c, l_c} \dot{\theta}_{j_c, h_c} (\mathbf{e}_{i_c, l_c} \times \mathbf{e}_{i,z})^T (\mathbf{e}_{j,x} \times \mathbf{e}_{j_c, h_c}) \right\} \\ & && : \text{Coriolis force term , } (j < i), n = [3, 2, 2] \end{aligned} \quad (\text{A43})$$

589

590 From Equations A40, A41 and A43, the vector $\dot{\mathbf{C}}\mathbf{V}$ can be divided into a centrifugal force component $\mathbf{D}_{\dot{\mathbf{C}}\mathbf{V}, \text{CNT}}$ and
591 a Coriolis force component $\mathbf{D}_{\dot{\mathbf{C}}\mathbf{V}, \text{COR}}$:

$$\dot{\mathbf{C}}\mathbf{V} = \mathbf{D}_{\dot{\mathbf{C}}\mathbf{V}, \text{CNT}} + \mathbf{D}_{\dot{\mathbf{C}}\mathbf{V}, \text{COR}} \quad (\text{A44})$$

592 Similarly, the vector $\dot{\mathbf{A}}\mathbf{V}$ can be decomposed into a centrifugal force component $\mathbf{D}_{\dot{\mathbf{A}}\mathbf{V}, \text{CNT}}$ and a Coriolis force
593 component $\mathbf{D}_{\dot{\mathbf{A}}\mathbf{V}, \text{COR}}$:

$$\dot{\mathbf{A}}\mathbf{V} = \mathbf{D}_{\dot{\mathbf{A}}\mathbf{V}, \text{CNT}} + \mathbf{D}_{\dot{\mathbf{A}}\mathbf{V}, \text{COR}} \quad (\text{A45})$$

594 The MDT contribution to the generalised acceleration vector is expressed as the sum of individual components
595 including the gyroscopic effect moment component $\mathbf{D}_{\dot{\mathbf{V}}, \text{MDT}, \text{GYRO}}$, the segment length fluctuation component

596 $\mathbf{D}_{\dot{\mathbf{V}}, \text{MDT}, \text{SG-FLCT}}$, the centrifugal force component $\mathbf{D}_{\dot{\mathbf{V}}, \text{MDT}, \text{CNT}}$ and the Coriolis force component $\mathbf{D}_{\dot{\mathbf{V}}, \text{MDT}, \text{COR}}$:

$$\mathbf{D}_{\dot{V},\text{MDT}} = \mathbf{D}_{\dot{V},\text{MDT,GYRO}} + \mathbf{D}_{\dot{V},\text{MDT,SG-FLCT}} + \mathbf{D}_{\dot{V},\text{MDT,CNT}} + \mathbf{D}_{\dot{V},\text{MDT,COR}},$$

$$\left\{ \begin{array}{l} \mathbf{D}_{\dot{V},\text{MDT,GYRO}} = \mathbf{S}_{\dot{V}} \mathbf{B}_{\text{sys}} \begin{bmatrix} \bar{\mathbf{H}} \mathbf{V} \\ \mathbf{0}_{9 \times 1} \\ \mathbf{0}_{2 \times 1} \end{bmatrix}, \quad \mathbf{D}_{\dot{V},\text{MDT,SG-FLCT}} = -\mathbf{S}_{\dot{V}} \mathbf{B}_{\text{sys}} \begin{bmatrix} \mathbf{0}_{18 \times 1} \\ \dot{\mathbf{C}}_B \mathbf{V} \\ \mathbf{0}_{2 \times 1} \end{bmatrix}, \\ \mathbf{D}_{\dot{V},\text{MDT,CNT}} = -\mathbf{S}_{\dot{V}} \mathbf{B}_{\text{sys}} \begin{bmatrix} \mathbf{0}_{18 \times 1} \\ \mathbf{D} \dot{\mathbf{c}}_{V,\text{CNT}} \\ \mathbf{D} \dot{\mathbf{a}}_{V,\text{CNT}} \end{bmatrix}, \quad \mathbf{D}_{\dot{V},\text{MDT,COR}} = -\mathbf{S}_{\dot{V}} \mathbf{B}_{\text{sys}} \begin{bmatrix} \mathbf{0}_{18 \times 1} \\ \mathbf{D} \dot{\mathbf{c}}_{V,\text{COR}} \\ \mathbf{D} \dot{\mathbf{a}}_{V,\text{COR}} \end{bmatrix} \end{array} \right. \quad (\text{A46})$$

597 Finally, the foot CG's speed can be obtained as the sum of the kinematically-decomposed components as follows:

$$s_{3,\text{MDT}}(k) = D_{s_{3,\text{MDT,GYRO}}}(k) + D_{s_{3,\text{MDT,SG-FLCT}}}(k) + D_{s_{3,\text{MDT,CNT}}}(k) + D_{s_{3,\text{MDT,COR}}}(k),$$

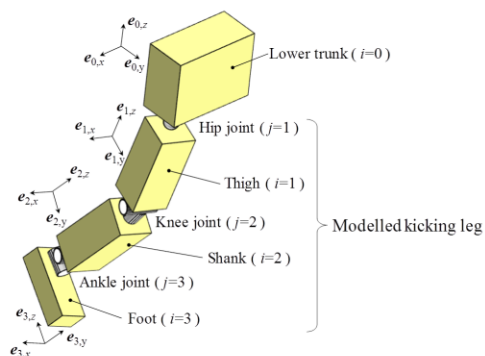
$$\left\{ \begin{array}{l} D_{s_{3,\text{MDT,GYRO}}}(k) = \mathbf{e}_3^T(k) \bar{\mathbf{S}}_3 \Delta t \sum_{h=0}^{k-1} \mathbf{D}_{\dot{V},\text{MDT,GYRO}}(h), \\ D_{s_{3,\text{MDT,SG-FLCT}}}(k) = \mathbf{e}_3^T(k) \bar{\mathbf{S}}_3 \Delta t \sum_{h=0}^{k-1} \mathbf{D}_{\dot{V},\text{MDT,SG-FLCT}}(h), \\ D_{s_{3,\text{MDT,CNT}}}(k) = \mathbf{e}_3^T(k) \bar{\mathbf{S}}_3 \Delta t \sum_{h=0}^{k-1} \mathbf{D}_{\dot{V},\text{MDT,CNT}}(h), \\ D_{s_{3,\text{MDT,COR}}}(k) = \mathbf{e}_3^T(k) \bar{\mathbf{S}}_3 \Delta t \sum_{h=0}^{k-1} \mathbf{D}_{\dot{V},\text{MDT,COR}}(h) \end{array} \right. \quad (\text{A47})$$

598 where $D_{s_{3,\text{MDT,GYRO}}}(k)$, $D_{s_{3,\text{MDT,SG-FLCT}}}(k)$, $D_{s_{3,\text{MDT,CNT}}}(k)$ and $D_{s_{3,\text{MDT,COR}}}(k)$ denote, respectively, the
599 components of the foot CG's speed at time k that arise from the gyroscopic effect moment, segment length
600 fluctuations, centrifugal forces and Coriolis forces.

601

602

603 Figure A1. A schematic representation of the modelled kicking leg introducing the numbering of the segments ($i=0$ to
604 3) and joints ($j= 1$ to 3), as well as the segmental coordinate systems.



605